

this document downloaded from

**vulcanhammer.net**

Since 1997, your complete online resource for information geotechnical engineering and deep foundations:

The Wave Equation Page for Piling

*Online books on all aspects of soil mechanics, foundations and marine construction*

Free general engineering and geotechnical software

*And much more...*

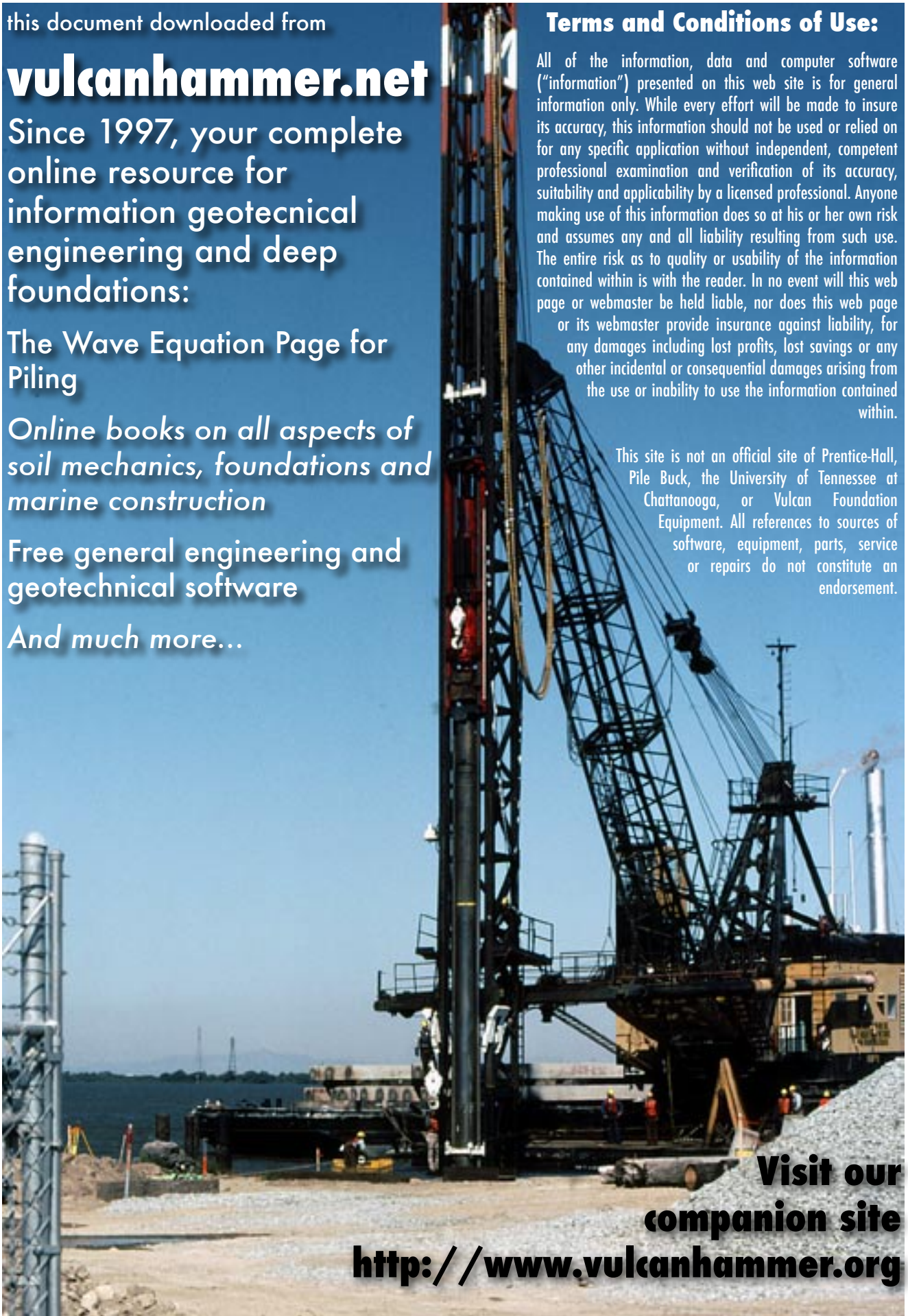
## Terms and Conditions of Use:

All of the information, data and computer software ("information") presented on this web site is for general information only. While every effort will be made to insure its accuracy, this information should not be used or relied on for any specific application without independent, competent professional examination and verification of its accuracy, suitability and applicability by a licensed professional. Anyone making use of this information does so at his or her own risk and assumes any and all liability resulting from such use. The entire risk as to quality or usability of the information contained within is with the reader. In no event will this web page or webmaster be held liable, nor does this web page or its webmaster provide insurance against liability, for any damages including lost profits, lost savings or any other incidental or consequential damages arising from the use or inability to use the information contained within.

This site is not an official site of Prentice-Hall, Pile Buck, the University of Tennessee at Chattanooga, or Vulcan Foundation Equipment. All references to sources of software, equipment, parts, service or repairs do not constitute an endorsement.

**Visit our  
companion site**

**<http://www.vulcanhammer.org>**





357

*STRESS DISTRIBUTION  
WITHIN AND UNDER  
LONG ELASTIC EMBANKMENTS*

*JUNE, 1967*

*NO. 14*

*by*

*W. H. PERLOFF  
G. Y. BALADI  
M. E. HARR*

*Joint  
Highway  
Research  
Project*

*PURDUE UNIVERSITY  
LAFAYETTE INDIANA*



Research Report

STRESS DISTRIBUTION  
WITHIN AND UNDER  
LONG ELASTIC EMBANKMENTS

To: Dr. G. A. Leonards, Director  
Joint Highway Research Project

June 20, 1967

File: 6-6-6

From: H. L. Michael, Associate Director  
Joint Highway Research Project

Project: CE-36-5F

The attached report entitled "Stress Distribution Within and Under Long Elastic Embankments" describes one phase of the project concerning long-term deformations of compacted cohesive soil embankments. The report was prepared by Professor W. H. Perloff, Research Engineer, Mr. G. Y. Baladi, Research Assistant, and Professor M. E. Harr.

The report presents diagrams of the distribution of stresses within and under long elastic embankments continuous with the foundation material. The significant differences in the magnitude and distribution of the stresses from those usually assumed are discussed.

Respectfully submitted,

*Harold L. Michael / WMP*

Harold L. Michael  
Associate Director

HLM:ms

Attachment

Copy: F. L. Ashbaucher	V. E. Harvey	M. B. Scott
W. L. Dolch	J. F. McLaughlin	W. T. Spencer
W. H. Goetz	F. E. Mendenhall	F. W. Stubbs
W. L. Grecco	R. D. Miles	H. R. J. Walsh
G. K. Mallock	J. C. Oppenlander	K. B. Woods
R. H. Harrell	C. F. Scholer	E. J. Yoder

Research Report

STRESS DISTRIBUTION  
WITHIN AND UNDER  
LONG ELASTIC EMBANKMENTS

by

W. H. Perloff, Associate Professor of Soil Mechanics  
G. Y. Baladi, Graduate Research Assistant  
M. E. Harr, Professor of Soil Mechanics

Joint Highway Research Project

Project: CE-36-5F

File: 6-6-6

Prepared as Part of an Investigation

Conducted by

Joint Highway Research Project  
Engineering Experiment Station  
Purdue University

in cooperation with the

Indiana State Highway Commission

and the

U.S. Department of Transportation  
Federal Highway Administration  
Bureau of Public Roads

The opinions, findings and conclusions expressed in this publication are those of the authors and not necessarily those of the Bureau of Public Roads.

Not Released for Publication

Subject to Change

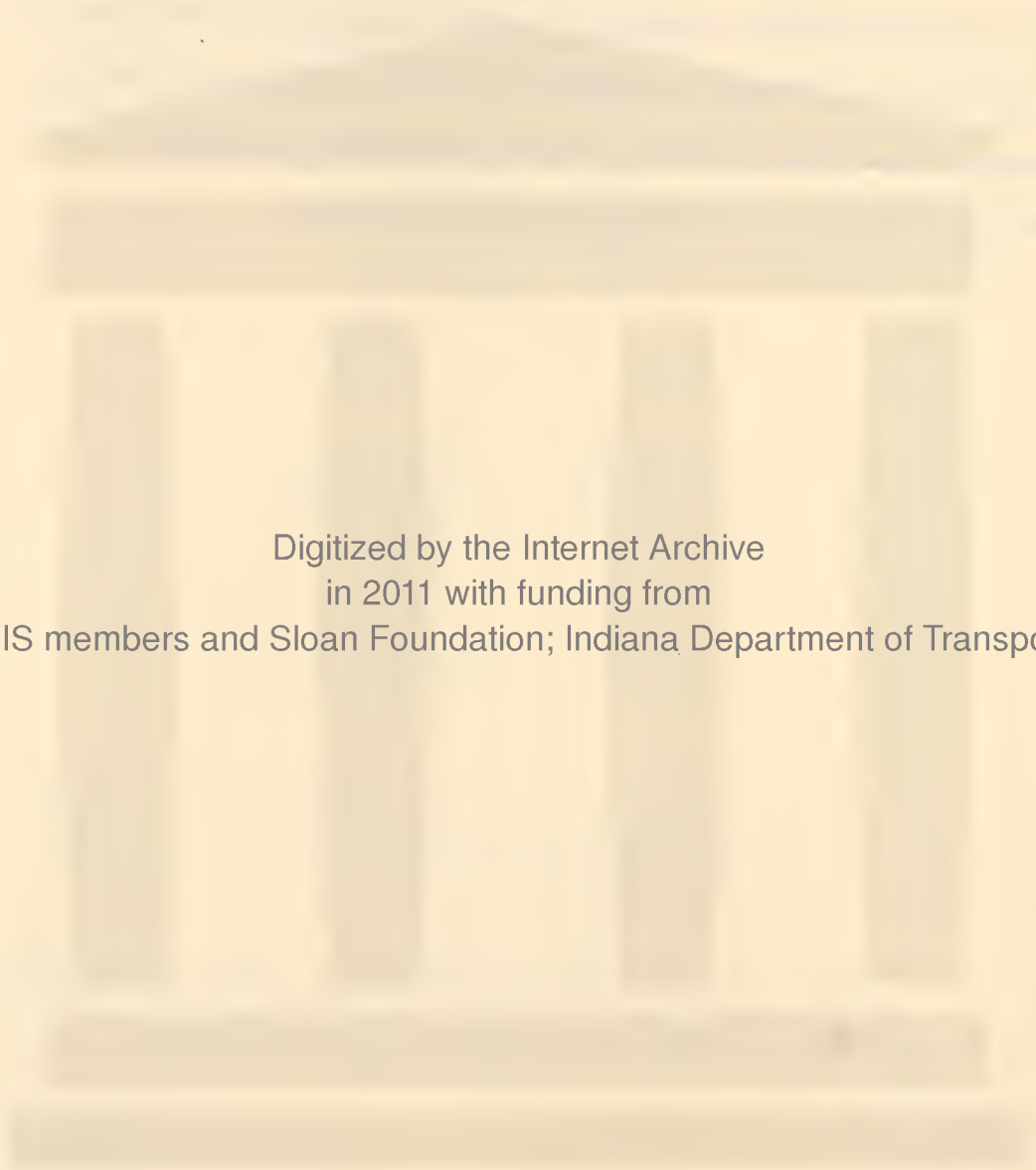
Not Reviewed By  
Indiana State Highway Commission  
or the  
Bureau of Public Roads

Purdue University  
Lafayette, Indiana  
June 20, 1967



## ABSTRACT

The distribution of stresses within and under long elastic embankments continuous with the underlying material is presented. The magnitude and distribution of stress in the foundation material in the vicinity of the embankment is significantly different from that predicted by the usual assumption of stress proportional to embankment height applied normal to the foundation. Influence charts for a variety of embankment shapes are given.



Digitized by the Internet Archive  
in 2011 with funding from  
LYRASIS members and Sloan Foundation; Indiana Department of Transportation

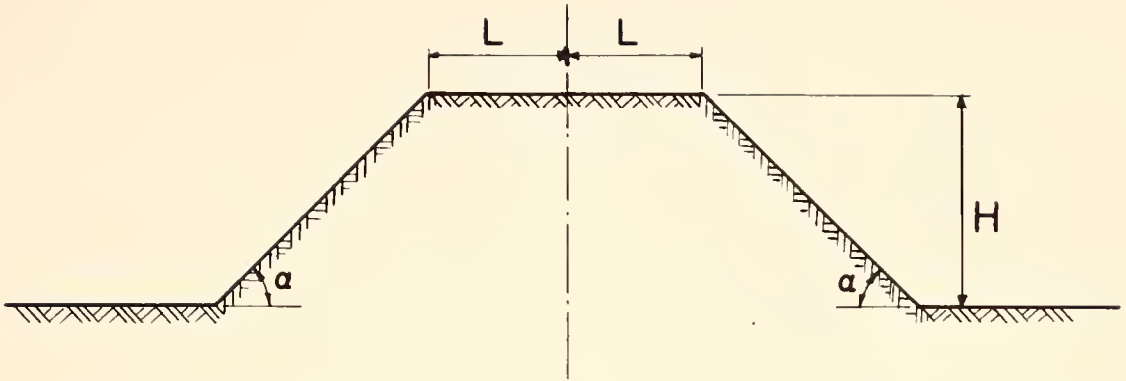
## INTRODUCTION

The distribution of stresses within and under earth embankments, due to the embankment weight, is of interest to civil engineers in a variety of applications. Consideration of deformations within embankments, analysis of stability, consolidation of underlying compressible materials, all require determination of the distribution of these stresses.

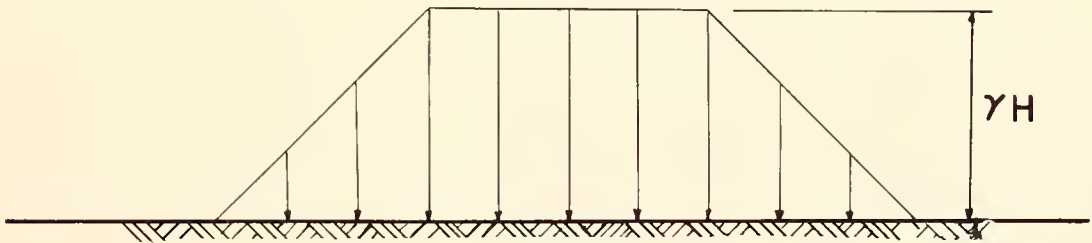
At the present time there is no means available by which a closed-form solution for such stresses can be obtained. Consequently, various approximations of the real problem have been made, with the objective of obtaining at least an estimate of the stresses. The first such effort was made by CAROTHERS (1920). He analyzed the stresses within an homogeneous, isotropic elastic half-space resulting from a "long embankment" loading. It was assumed that the load was applied normal to the boundary with a magnitude proportional to the height of the embankment. These results were presented in tabular form by JURGENSON (1937). OSTERBERG (1957) superimposed solutions given by NEWMARK (1940, 1942) to develop an influence chart for the determination of the magnitude of vertical stresses induced in an elastic half-space by a long embankment loading with a variety of cross sections. Again, the magnitude of the pressure was assumed to be proportional to the embankment height and applied normal to the surface of the foundation material. This "normal loading approximation" to the actual embankment loading is illustrated in Figure 1a.

TERZAGHI (1943) described an effort to evaluate the shear stresses transmitted to the foundation material by an embankment made by RENDULIC





(a) Long Symmetric Elastic Embankment  
Continuous With Foundation



(b) Normal Loading Approximation

Fig. 1 - Problem Considered

(1936). It was assumed that the embankment material was on the verge of failure and thus the shearing resistance of the embankment was fully mobilized in order to maintain equilibrium. Consequently, TERZAGHI (1943) suggested that the magnitude of the computed shear stress at the base was likely to be lower than the actual in-situ stresses.

TROLLOPE (1957), and DAVIS and TAYLOR (1962) considered the state of stress within a granular embankment resting on a foundation which yielded an arbitrary amount. No attempt was made to compute the amount of foundation movement which would be created by the embankment.

FINN (1960) suggested the use of the Schwarz-Christoffel transformation to map the embankment surface into a straight line, thereby utilizing the distribution of stresses within a semi-infinite elastic medium. However, he did not carry out the suggested procedure.

Numerical methods have been used to obtain, for particular cases, solutions for the stress distribution in an elastic embankment resting on elastic or rigid foundations. ZIENKIEWICZ (1947) used a finite difference approach to analyze the stress distribution within a triangular gravity dam resting on an elastic foundation. This was extended by ZIENKIEWICZ and GERSTNER (1961) to the case in which the foundation modulus differed from that of the dam. DINGWALL and SCRIVNER (1954) applied the method of finite differences to the solution of an embankment on a rigid foundation. CARLTON (1962) used a similar method to study an elastic embankment continuous with an elastic foundation.

The finite element method of numerical analysis has been applied by ZIENKIEWICZ and CHEUNG (1964, 1965) in the study of stresses within buttress dams resting on elastic foundations. CLOUGH and CHOPRA (1966) and

FINN (1966), respectively, have also applied the finite element method to the study of a triangular dam on a rigid foundation and a rock slope continuous with its elastic foundation.

BROWN (1962) and GOODMAN and BROWN (1963) investigated the case of a long elastic slope constructed incrementally; it is not clear to what degree their results are influenced by the fact that compatibility is not satisfied by their solution method.

In each of the cases approached by numerical methods, the solution was either restricted to a single embankment cross section or a complete stress picture was not obtained. Thus, despite numerous attempts to determine the distribution of stresses within and under an embankment, no closed-form solution is presently available. It is the objective of this paper to present such a solution.

#### PROBLEM CONSIDERED

The problem considered herein is the determination of the distribution of stresses within and under an embankment resulting from the self-weight of the embankment. The embankment is shown schematically in Figure 1b. It is assumed that the embankment and the foundation material with which it is continuous, are composed of homogeneous, isotropic, linear elastic material. Further, the embankment is assumed to be sufficiently long so that plane strain conditions apply. The shape of the symmetric cross section is defined by the slope angle  $\alpha$  and the ratio of the half-width of the top of the embankment,  $L$ , to the embankment height,  $H$ .

The solution is obtained by transforming the region of the embankment where the solution is unknown, into a half-space where the solution can be

found. Application of the Cauchy integral formula to the boundary conditions permits determination of the stresses. An outline of the method is given in Appendix 1.

## RESULTS AND DISCUSSION

### Vertical Normal Stress

A typical result is illustrated in Figure 2. This figure shows contours of the vertical normal stress in dimensionless form,  $\sigma_y/\gamma H$ , for an embankment with  $\alpha = 45^\circ$ ,  $L/H = 3$ , and Poisson's ratio,  $\mu = 0.3$ . The contour lines show only the effect of the embankment weight. Thus, at depths below the base of the embankment ( $y/H = 0$ ) the material is assumed weightless. The effect of the medium weight can be superimposed upon these values to give the total stress acting at a point. The two dashed lines in Figure 2 show stress contours, in terms of  $\sigma_y/\gamma H$ , for the usual normal loading approximation corresponding to this embankment. These indicate that the vertical normal stresses produced in the foundation material below the elastic embankment are generally smaller than computed for the normal loading approximation.

The stress distribution due to the normal loading approximation is independent of Poisson's ratio; the stresses due to the elastic embankment are dependent upon  $\mu$ . However, the vertical stresses are insensitive to its magnitude; changing  $\mu$  from 0.3 to 0.5 changes the vertical stress at a point by less than five per cent.

The effect of embankment shape on the vertical stress along vertical sections through the center line of the embankment and the toe of the slope,



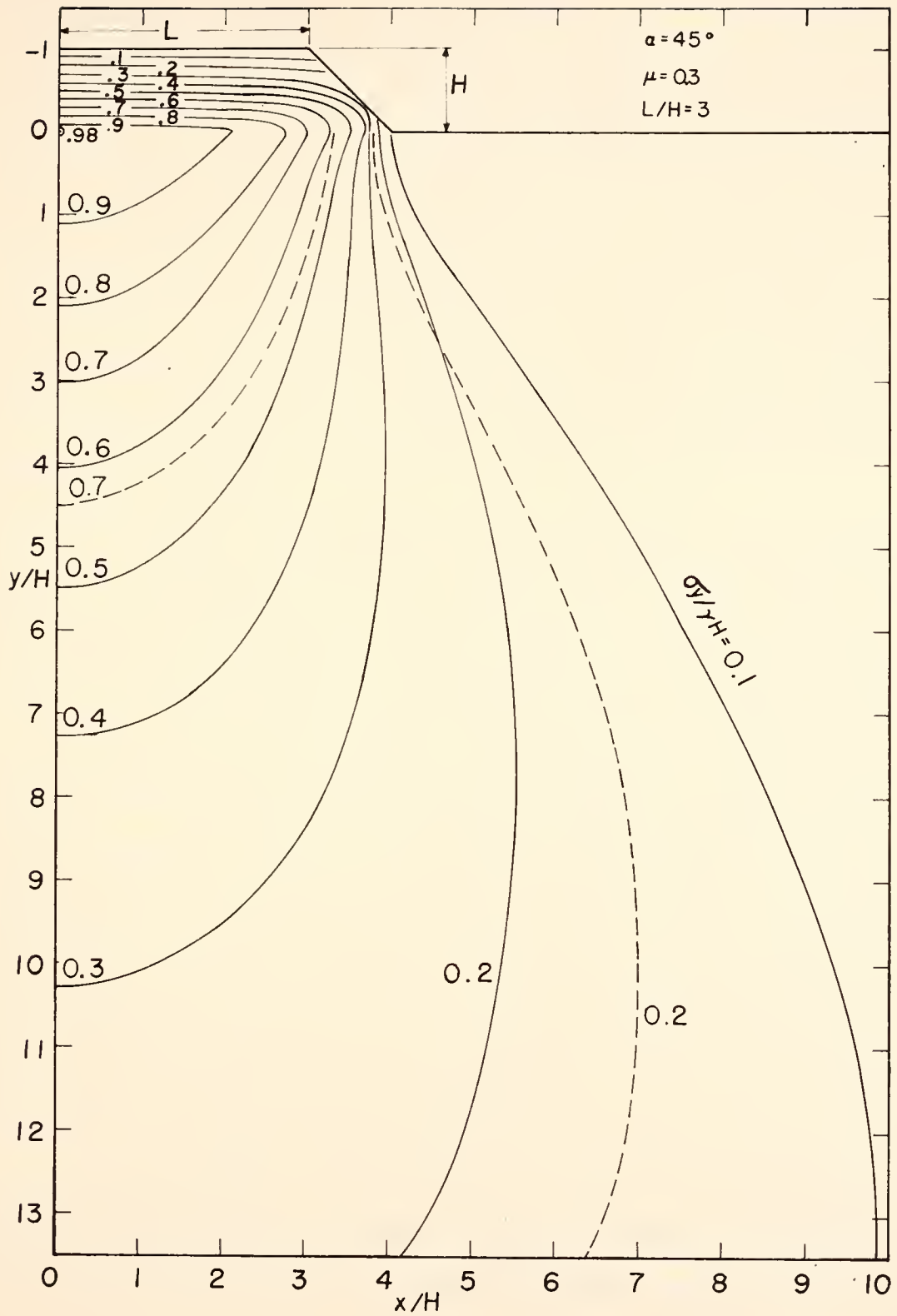


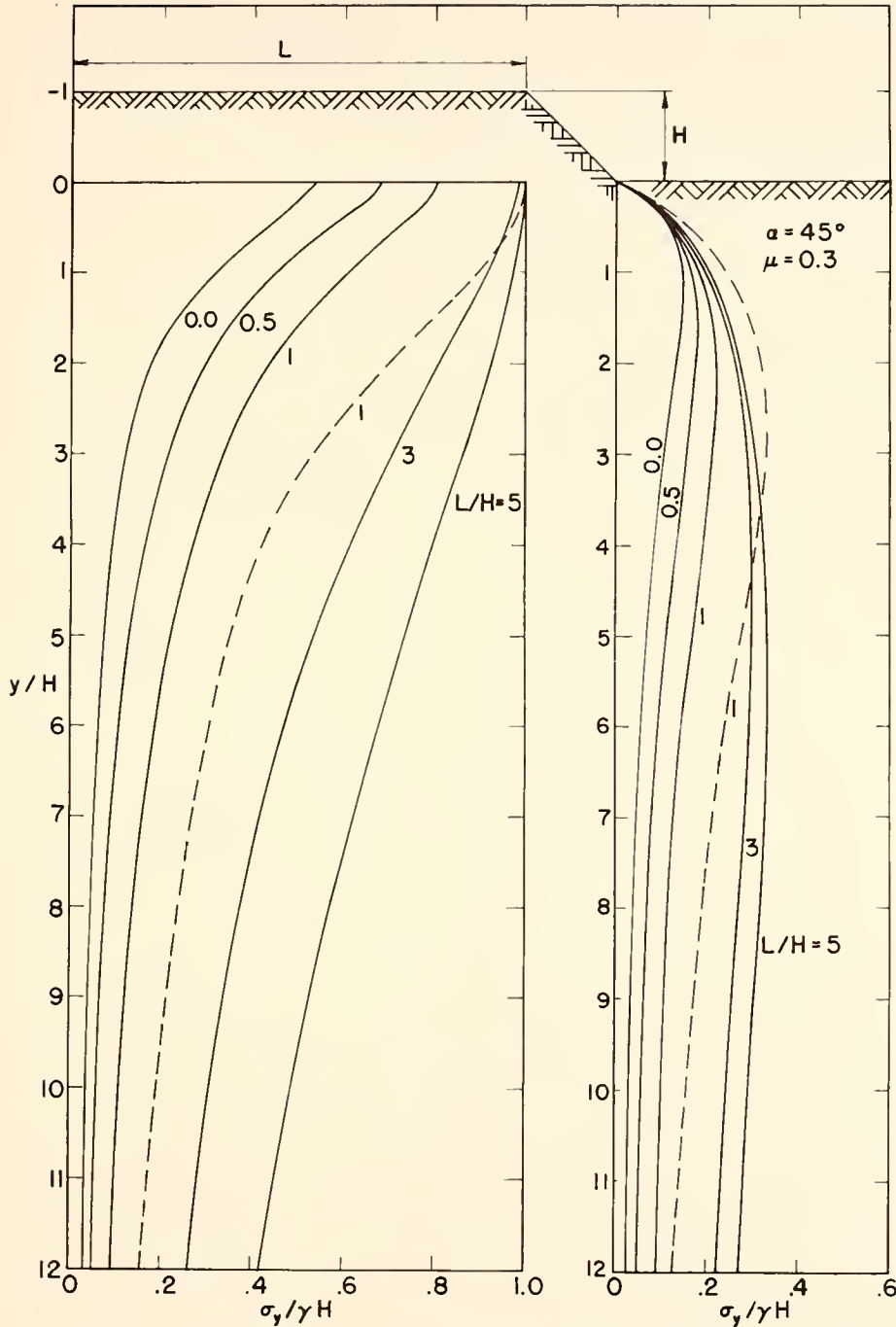
Fig. 2-Contours for Vertical Stress

is illustrated in Figure 3, for  $\alpha = 45^\circ$  and  $\mu = 0.3$ . The figure is a composite diagram showing the embankment schematically, and the magnitude of the vertical stress at each section as a function of depth. Clearly, the L/H ratio has a pronounced effect on the distribution of vertical stress. As L/H decreases, the stress decreases. Furthermore, a smaller L/H ratio produces a more rapid dissipation of stress with depth.

The dashed lines show the vertical normal stress for the normal loading approximation equivalent in shape to the embankment for which L/H = 1. As indicated in Figure 2, the vertical stress for the corresponding elastic embankment is smaller.

Figure 4 shows the distribution of vertical normal stress along the base of the embankment for  $\mu = 0.3$ , four values of  $\alpha$ , and several embankment shapes shown schematically in the figure. The curved solid lines represent the distribution of stress against the base; dashed lines show the distribution of stress assumed in the usual normal loading approximation. The stress distribution is much more uniform under the elastic embankment than is ordinarily assumed. The difference becomes especially apparent as the L/H ratio of the steeper embankments decreases. Moreover, the magnitude of the stress under the central zone of the elastic embankment is less than that shown by the dashed curves. Again the effect is enhanced for narrow, steep embankments (for  $\alpha = 45^\circ$  and L/H = 0 the vertical stress is only 65 per cent of that usually assumed).

In order to satisfy equilibrium, the areas under corresponding dashed and solid curves must be the same. Hence the difference between these curves becomes less pronounced, at least near the central portion of the embankment,



(a) At Centerline      (b) At Toe of Slope

Fig. 3 - Distribution of Vertical Stress Along Vertical Sections for Varying  $L/H$  Ratios

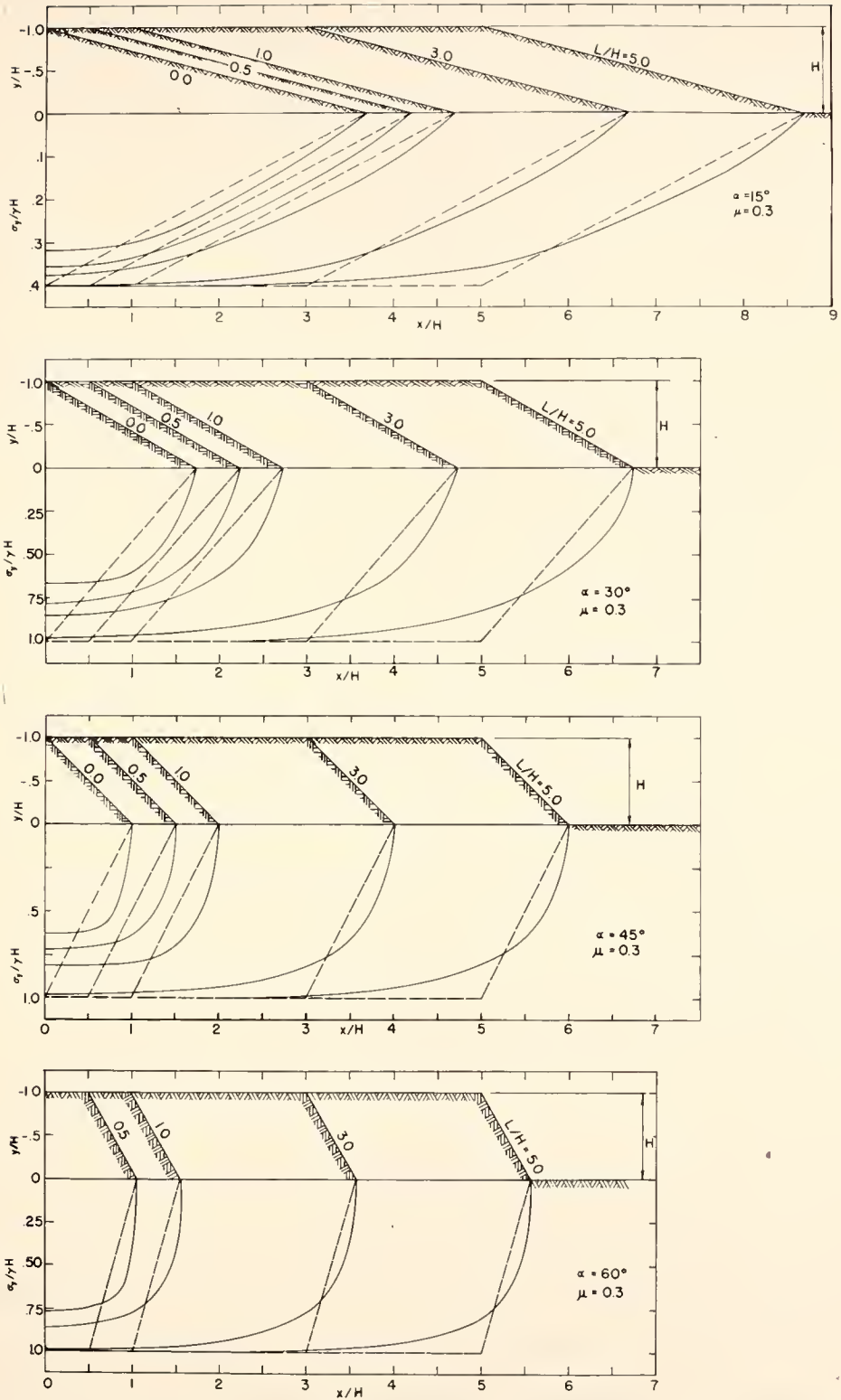


Fig. 4 - Distribution of Vertical Normal Stress,  $\sigma_v/\gamma H$  On The Base of The Embankment For Varying  $\alpha$ , And  $L/H$  Ratios



as  $L/H$  increases. However, near the outer edge of the embankment, the stresses are still significantly larger on a proportional basis, than indicated by the normal loading approximation. Thus, for embankments with moderate  $L/H$  ratios, the normal loading approximation leads to larger estimates of differential settlement, assuming one-dimensional compression, than would be computed by the method presented herein.

#### Horizontal Normal Stress

Contours of horizontal normal stress,  $\sigma_x/\gamma H$ , for  $\alpha = 45^\circ$ ,  $L/H = 3$  and  $\mu = 0.3$  are shown in Figure 5. The dashed lines are contours determined from the usual normal loading approximation. The stresses shown are those due to the embankment only. The figure shows that the maximum horizontal stress occurs within the body of the embankment and decreases with increasing depth. In the foundation material in the vicinity of the elastic embankment,  $\sigma_x/\gamma H$  is less than half of that usually assumed.

The effect of embankment shape on the horizontal stress along vertical sections through the center line of the embankment and the toe of the slope, is illustrated in Figure 6 for  $\alpha = 45^\circ$  and  $\mu = 0.3$ . As the embankment becomes narrower ( $L/H \leq 1$ ), the stress is actually negative at some points below the center line. That is, the embankment causes a reduction in horizontal stress at these points.

The dashed line shows the stresses determined from the normal loading approximation for  $L/H = 1$ . The stress is larger than that due to the elastic embankment at all depths. In fact, in the vicinity of the embankment it is more than five times as large under the center line and twice as large under the toe. In contrast to the elastic embankment, the normal loading

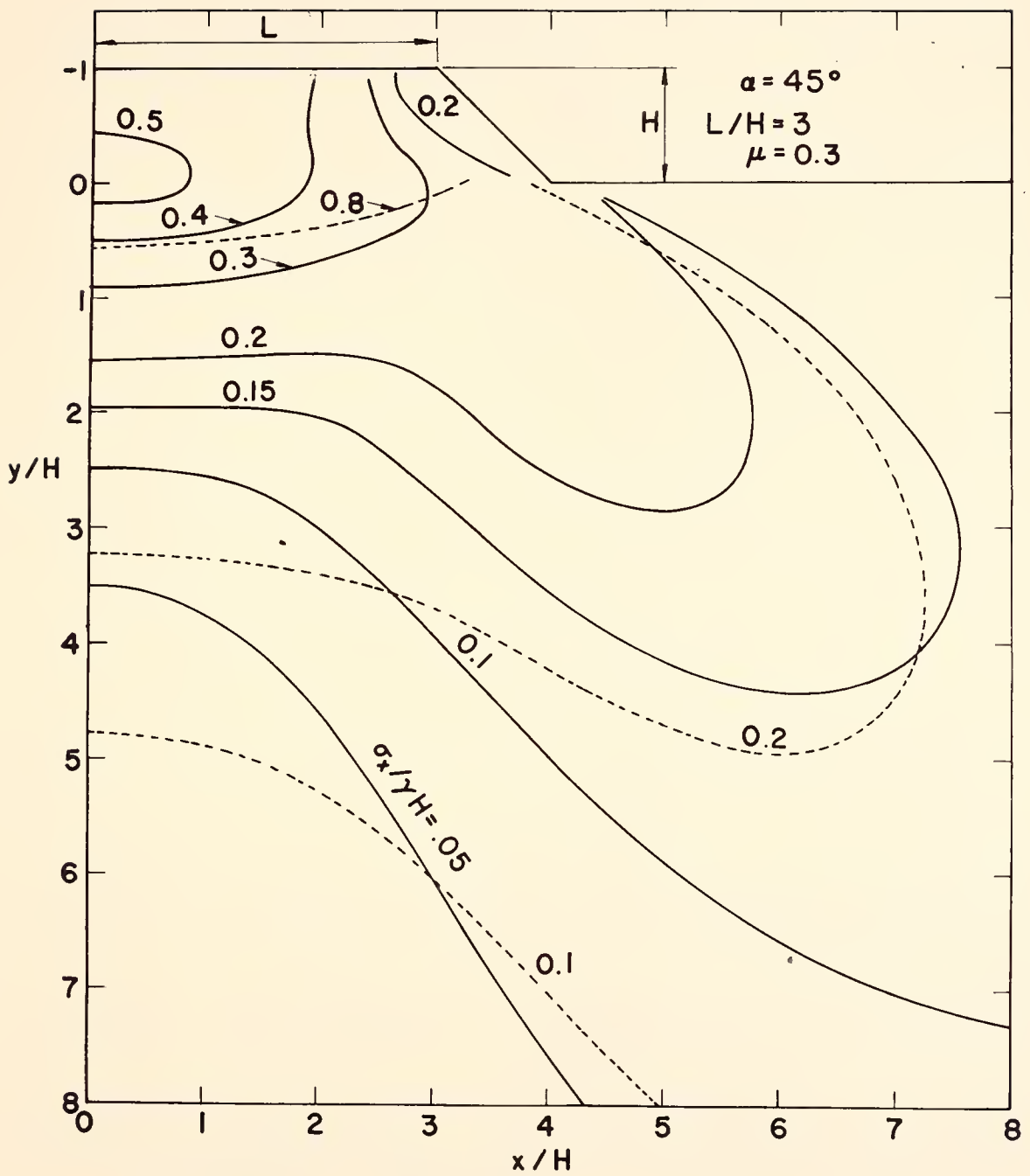
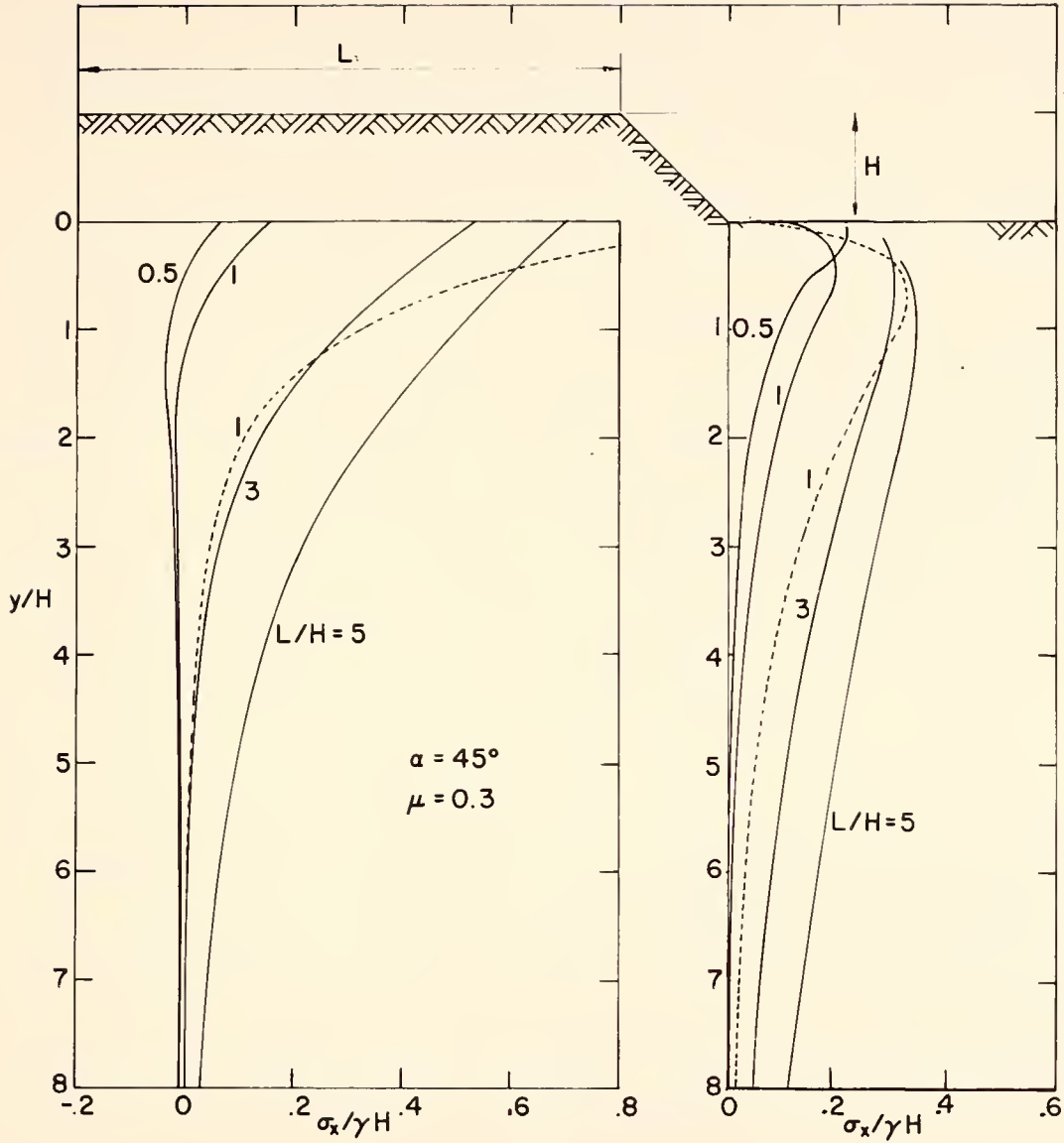


Fig. 5- Contours for Horizontal Stress



(a) At Centerline

(b) At Toe of Slope

Fig. 6-Distribution of Horizontal Stress Along Vertical Sections for Varying  $L/H$  Ratios

approximation does not produce negative horizontal stress at any depth. The reason for this difference becomes apparent when the shear stresses transmitted by the embankment to the foundation material are considered. This is discussed below.

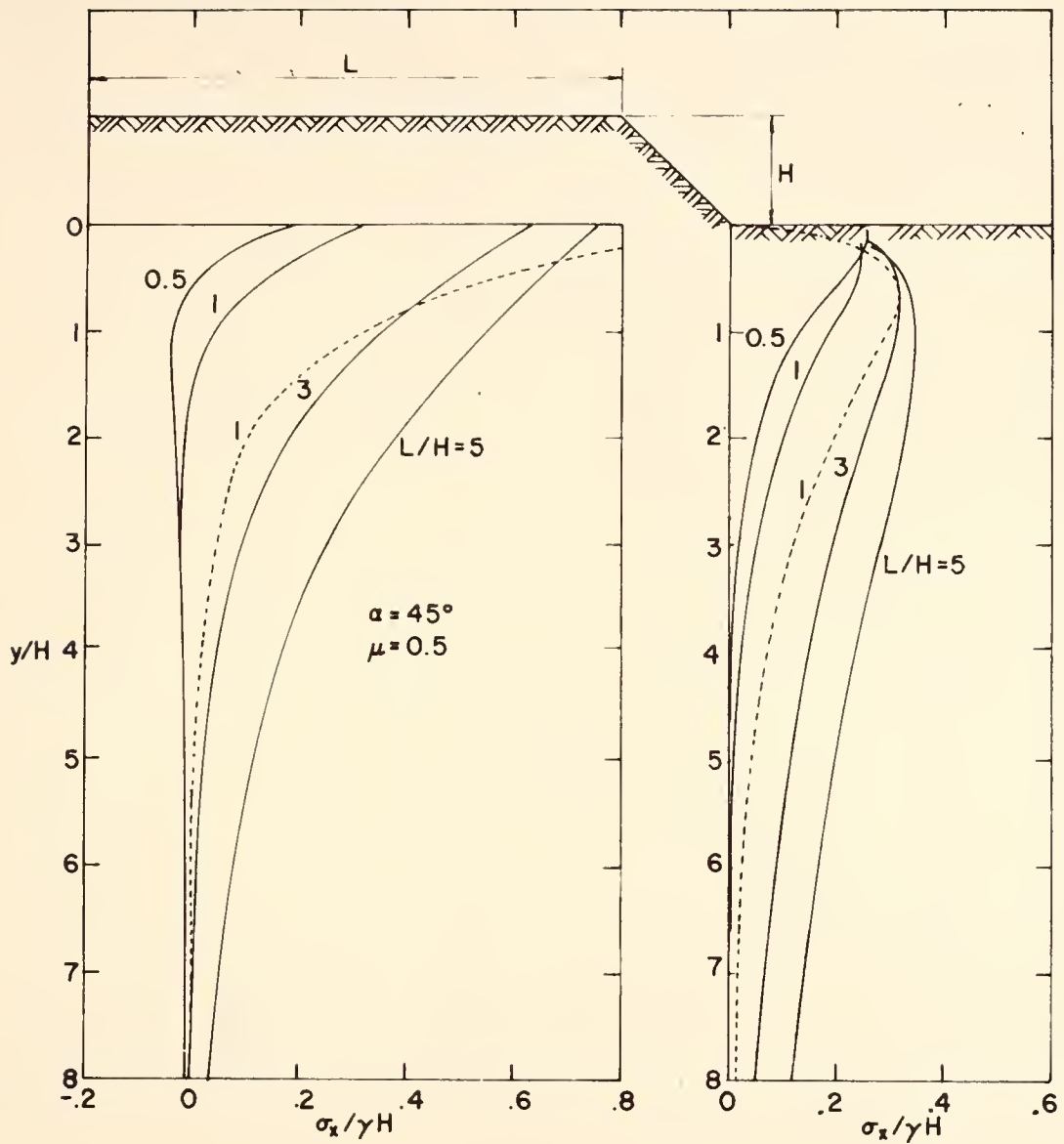
The effect of Poisson's ratio on the horizontal stress is illustrated in Figure 7. This figure shows the horizontal stress along vertical sections through the centerline and toe of the embankment for  $\alpha = 45^\circ$  and  $\mu = 0.5$ . The dashed line shows the stress due to the normal loading approximation for  $L/H = 1$ . Comparison with Figure 6 indicates that a change in Poisson's ratio from 0.3 to 0.5 changes the stress at shallow depths below the central portion of the embankment by as much as a factor of three. The difference decreases as the  $L/H$  ratio increases. The influence of  $\mu$  is less pronounced below the toe than below the center line.

#### Horizontal and Vertical Shear Stress

Contours of horizontal and vertical shear stress,  $\tau_{xy}/\gamma H$ , are shown in Figure 8, for  $\alpha = 45^\circ$  and  $L/H = 3$ . The solid contours are for Poisson's ratio of 0.3. The long dashed contours are for  $\mu = 0.5$ , and short dashed lines are for the normal loading approximation. The figure indicates the existence of horizontal shear stresses within the body of the embankment, increasing to a value at the base near the toe of the slope, in excess of  $0.2 \gamma H$ . However, the maximum value of horizontal shear stress (approximately  $0.3 \gamma H$ ) occurs below the base of the embankment.

Like the horizontal normal stress, the shear stress,  $\tau_{xy}$ , is affected markedly by the magnitude of Poisson's ratio. However, the effect observed depends upon the position of the point considered, relative to the base of





(a) At Centerline (b) At Toe of Slope

Fig. 7—Distribution of Horizontal Stress Along Vertical Sections for Varying  $L/H$  Ratios

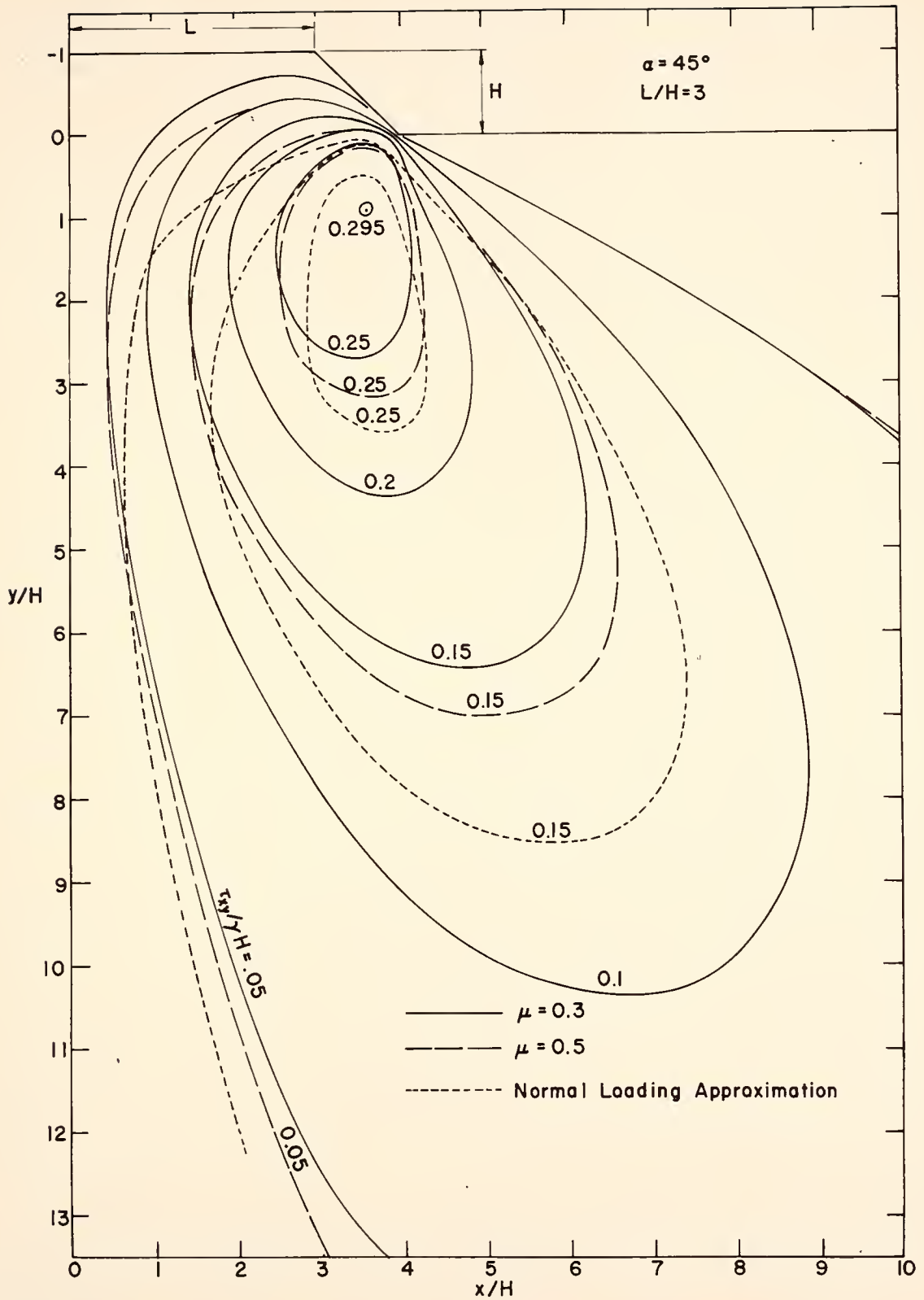


Fig. 8- Contours of Shear Stress,  $T_{xy}$

the embankment. In the zone below the embankment to a depth of  $y/H$  equal approximately two or three, the shear stresses in the incompressible material ( $\mu = 0.5$ ) are less than for the case in which  $\mu = 0.3$ . At greater depths, the reverse is true. The shear stress determined from the normal loading approximation is less than that for either  $\mu$  above a depth factor of approximately three to five, and more at greater depths. The magnitude of this effect depends upon the horizontal location considered, as shown in the figure.

The normal loading approximation assumes that there is no shear stress at the base of the embankment. Figures 8 and 9 indicate that, for the elastic embankment, this assumption is not reasonable. Figure 9 shows the horizontal shear stress,  $\tau_{xy}/\gamma H$ , at the base of the embankment for  $\mu = 0.3$ , four values of  $\alpha$ , and a variety of embankment shapes shown schematically in the figure. The horizontal shear stress is zero at the centerline, as required by symmetry, and reaches a maximum near the toe of the slope. The magnitude of the maximum and its location depend upon  $\alpha$  and the embankment shape. As  $L/H$  decreases for a given  $\alpha$ , the maximum  $\tau_{xy}/\gamma H$  increases, and moves closer to the toe of the slope. The magnitude of the increase is slight for  $\alpha = 15$  degrees, but becomes more significant as  $\alpha$  increases. Note that a maximum  $\tau_{xy}/\gamma H$  in excess of 0.4 implies that the horizontal shear stress at the base of a forty foot high embankment may be greater than one ton per square foot (unless the shear strength of the material is such that failure is induced).

To assist the designer in evaluating the significance of these results to his particular problem, influence diagrams for vertical normal, horizontal normal and shear stress distribution for a variety of cases are presented in Appendix 2.

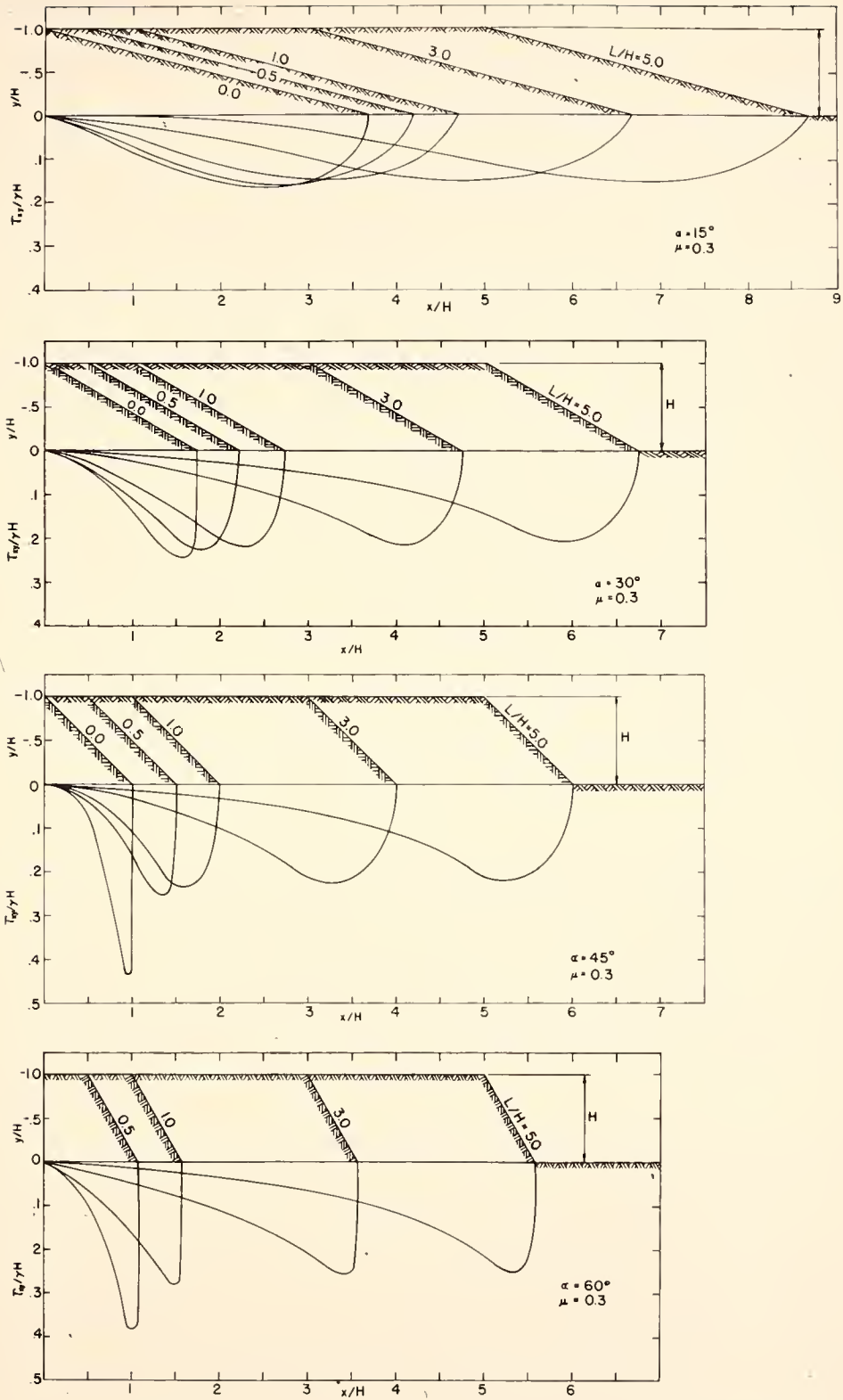


Fig. 9 - Distribution of Shear Stress,  $T_{xy}/\gamma H$  On The Base of The Embankment For Varying  $\alpha$ , And  $L/H$  Ratios



### Maximum Shear Stress

It is often useful to consider whether the maximum (i.e., principal) shear stress,  $\tau_{\max}/\gamma H$ , at any depth beneath the embankment exceeds the available shear strength. Thus, it is desirable to know the magnitude and distribution of maximum shear stresses due to the embankment. Contours of  $\tau_{\max}/\gamma H$  are shown in Figure 10 for the embankment section of Figures 2, 5 and 8. Note that the magnitude of  $\tau_{\max}$  transmitted from the embankment to the foundation material is approximately  $0.25 \gamma H$  at the base of the embankment in the vicinity of the toe. However, the largest shear stress,  $0.33\gamma H$ , occurs beneath the center line at  $Y/H = 1.8$ . It is also interesting to observe that within the embankment, the maximum shear stresses are larger near the top than in the mid-depth region, and that they increase again as depth increases. This is believed due to the relatively large horizontal stresses which are induced by the deformation mode of the embankment (cf. Figure 5).

Two contours of  $\tau_{\max}/\gamma H$  for the normal loading approximation corresponding to the embankment considered are shown in Figure 10 as dashed lines. They indicate a shear stress less than that produced by the elastic embankment in a shallow zone below the embankment, but larger shear stresses at depth.

Data for a variety of embankment shapes, with  $\mu = 0.3$ , and  $\alpha = 15^\circ$ ,  $30^\circ$ ,  $45^\circ$ ,  $60^\circ$  and  $75^\circ$  are shown in Figures 11 to 15, respectively. In these figures, the maximum value of  $\tau_{\max}$  at a particular depth is plotted as a function of depth for various  $L/H$  ratios. The horizontal location of the point at which this maximum value occurs is also shown. It can be

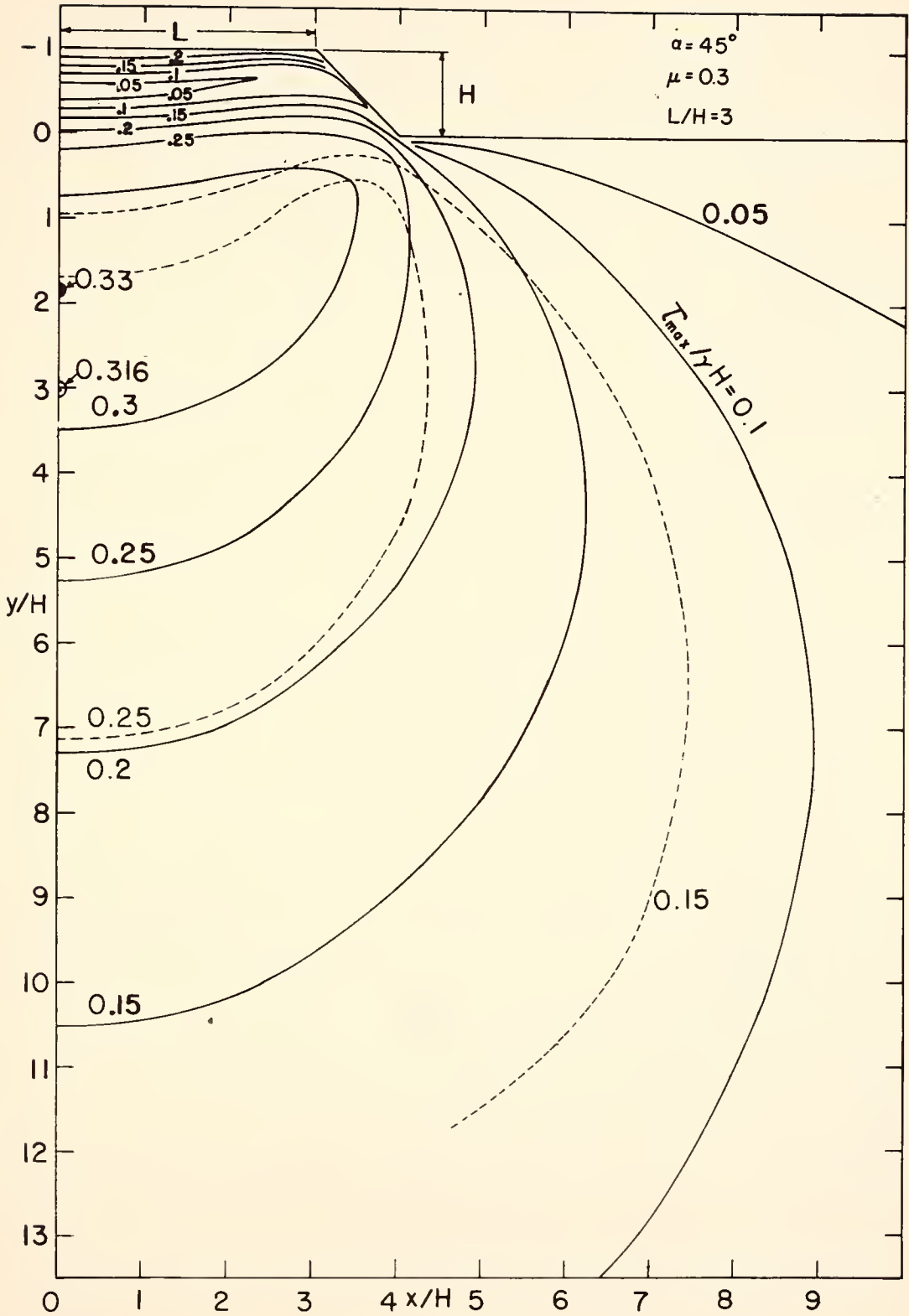


Fig.10-Contours for Max. Shear,  $T_{max}/\gamma H$

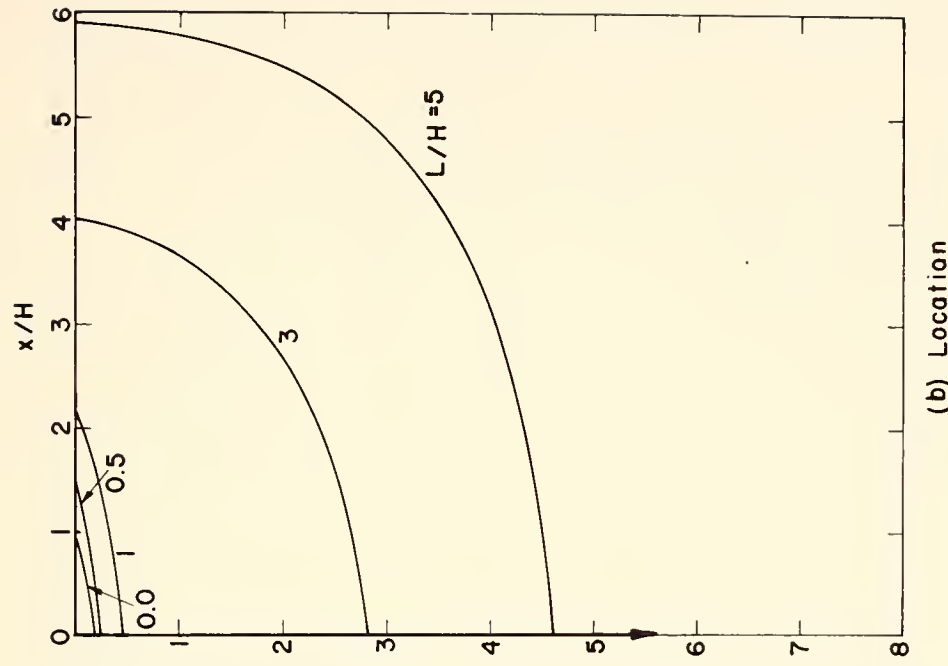
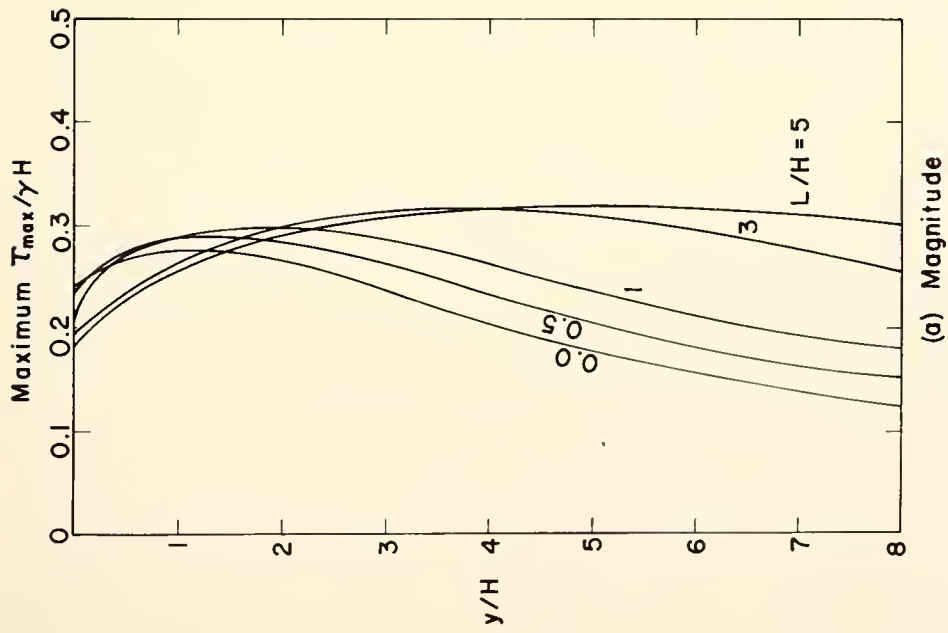
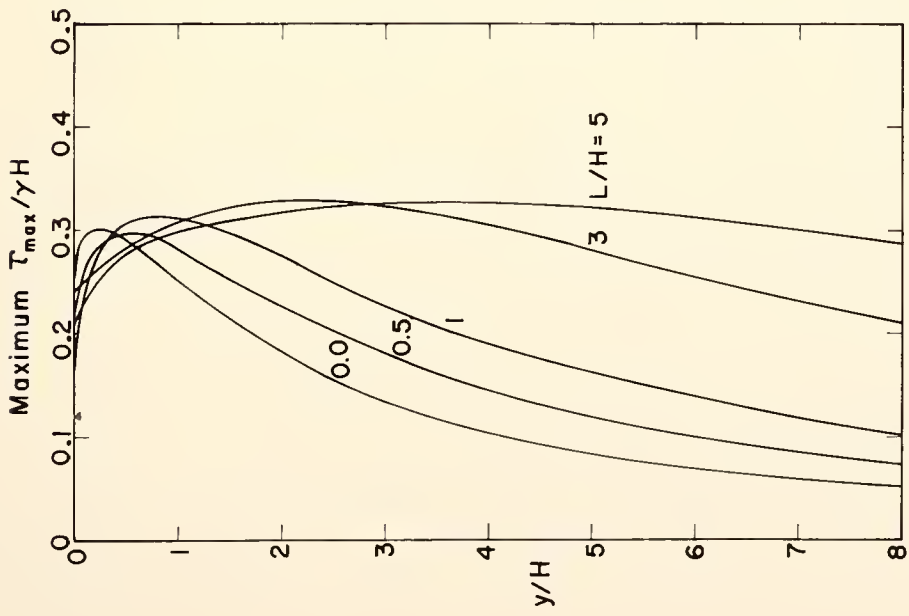
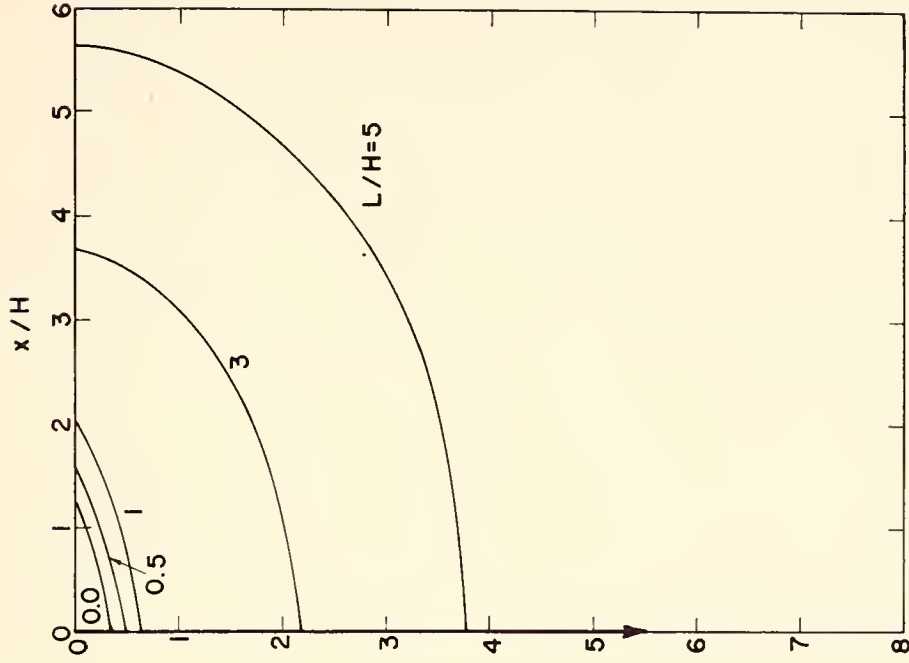


Figure 11-Magnitude and Location of Maximum ( $T_{max}/\gamma H$ ) as a Function of Depth for  $\mu=0.3$ ,  $\alpha = 15^\circ$



(a) Magnitude



(b) Location

Figure 12 - Magnitude and Location of Maximum  $(\tau_{max}/\gamma H)$  as a Function of Depth for  $\mu = 0.3$ ,  $\alpha = 30^\circ$



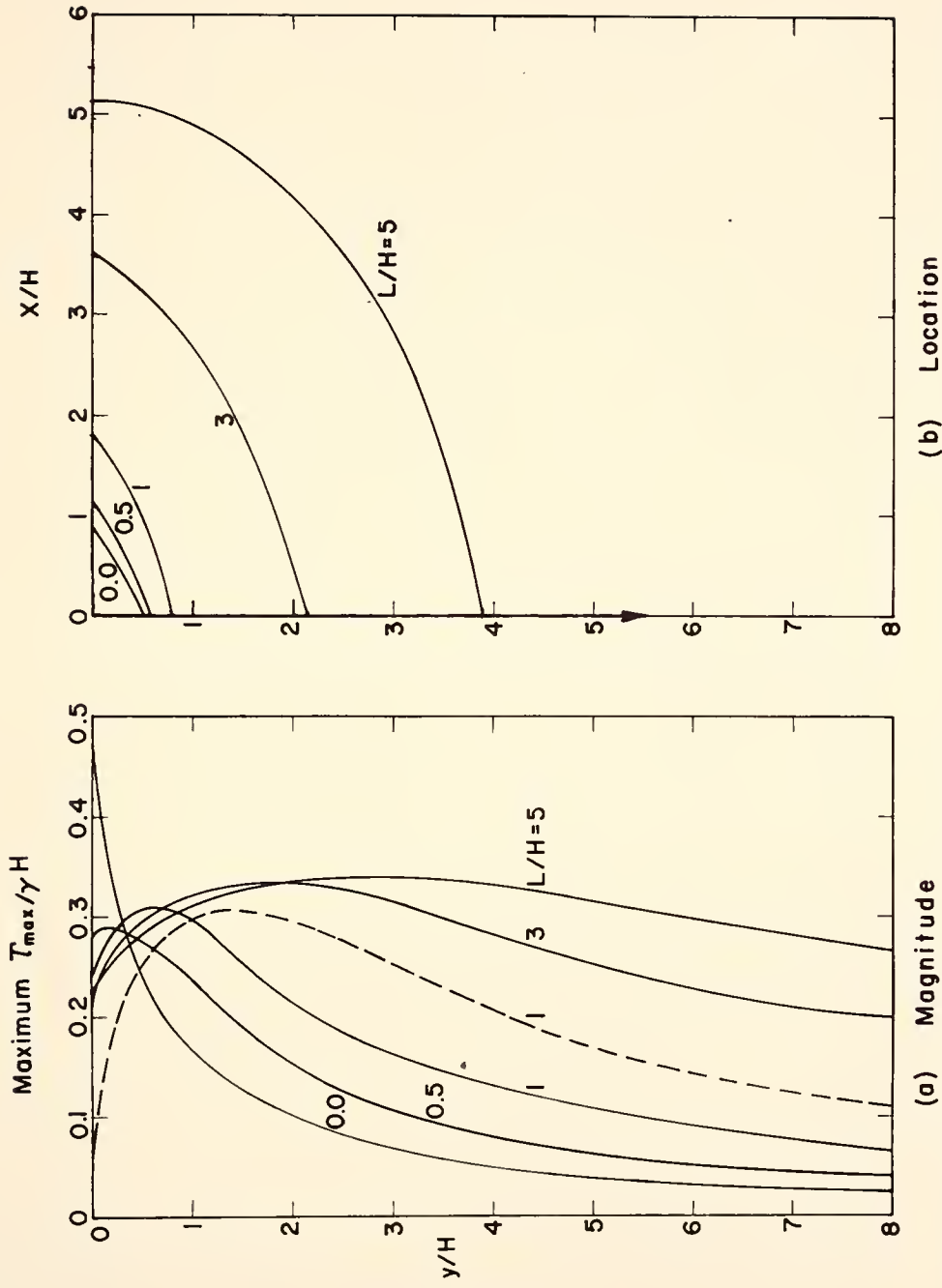


Figure 13 - Magnitude and Location of Maximum  $(T_{max}/\gamma H)$  as a Function of Depth for  $\alpha = 45^\circ$ .

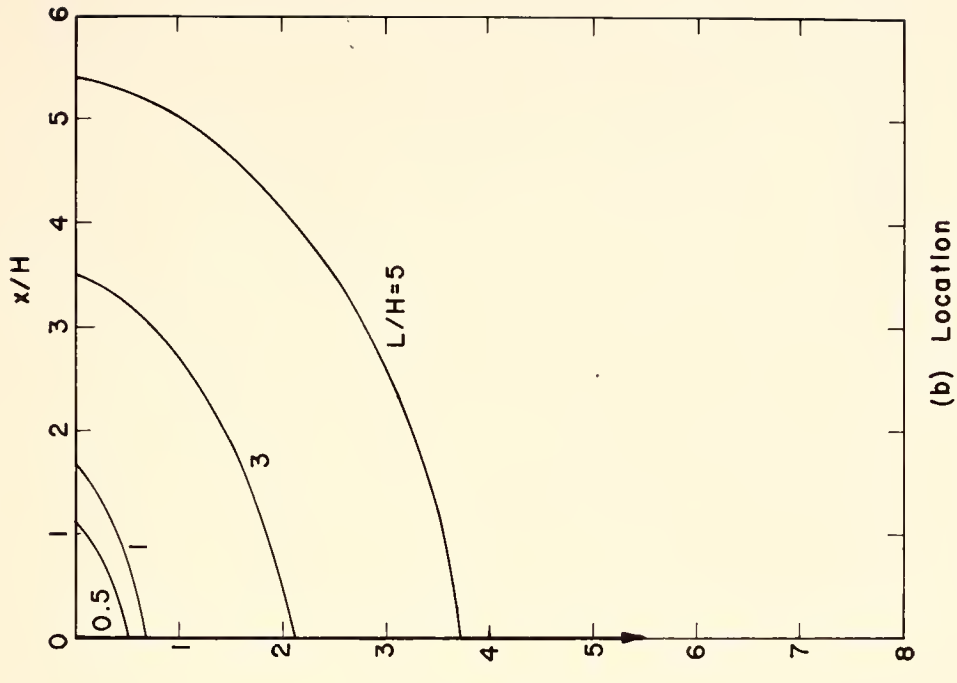
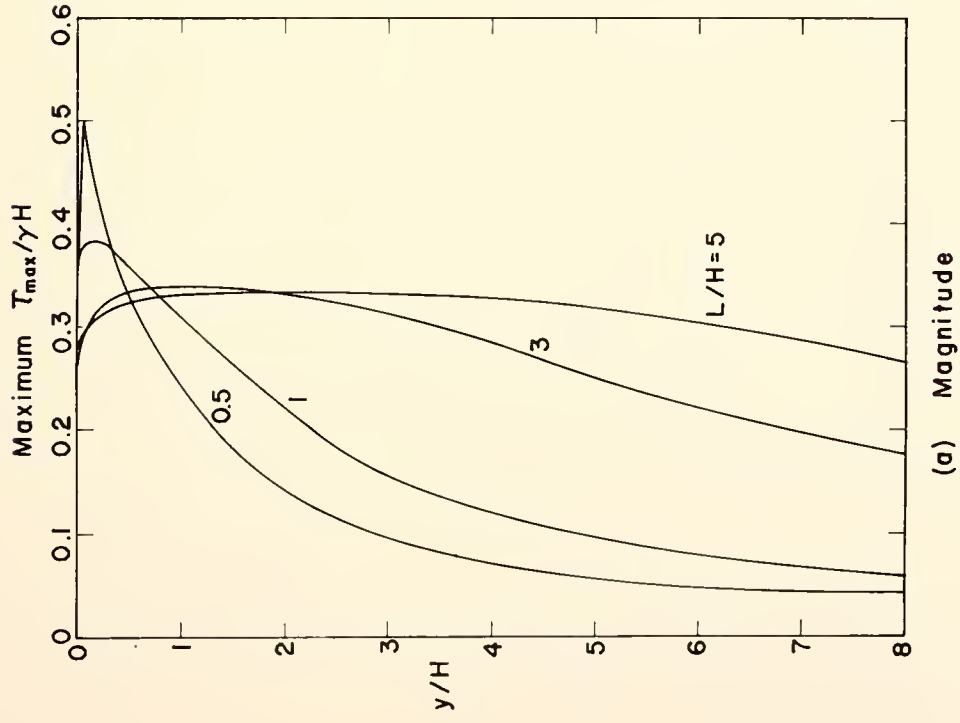


Figure 14 - Magnitude and Location of Maximum  $(T_{max}/\gamma H)$  as a Function of Depth for  $\mu = 0.3$ , and  $\alpha = 60^\circ$

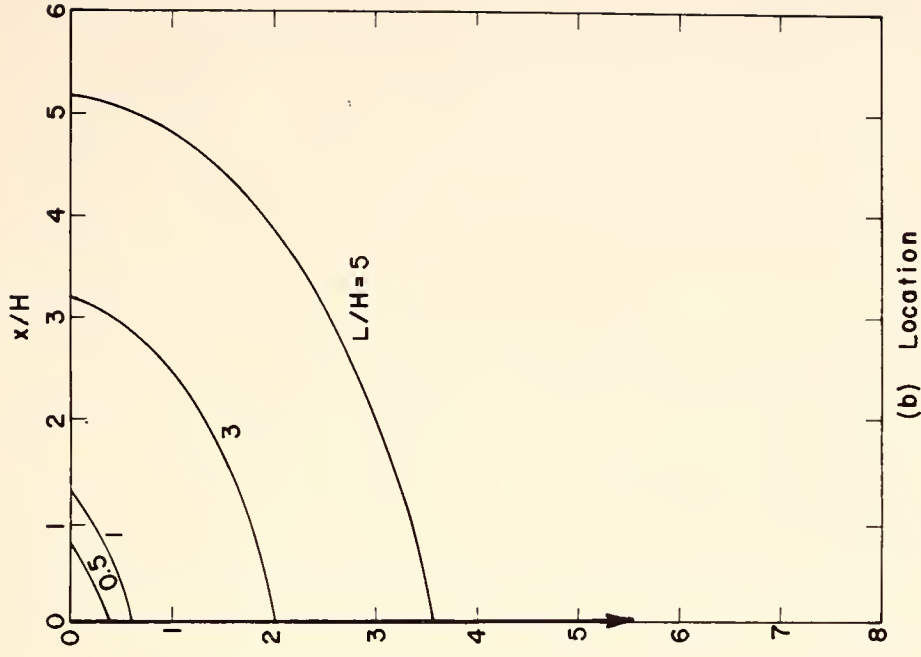
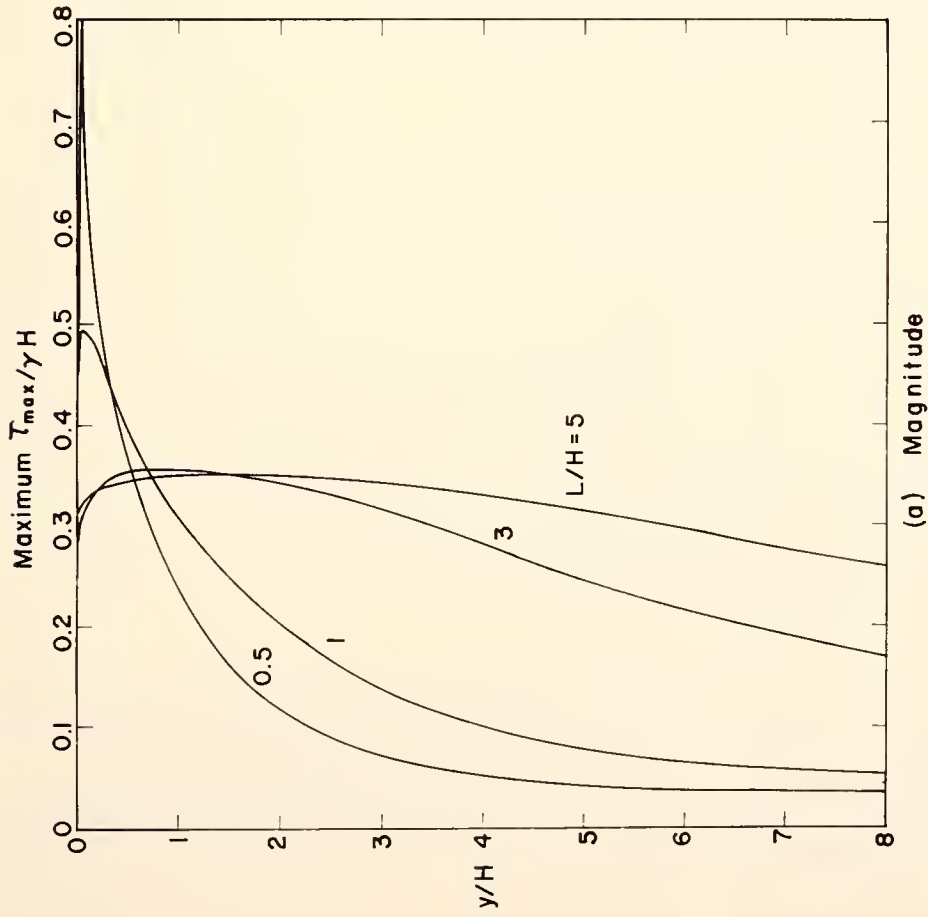


Figure 15 - Magnitude and Location of Maximum  $(T_{\max}/\gamma H)$  as a Function of Depth for  $\mu = 0.3$  and  $\alpha = 75^\circ$

observed that in Figure 11, that as the L/H ratio increases for  $\alpha = 15^\circ$ , peak  $\tau_{\max}$  increases in magnitude, and acts at an increasing depth below the embankment. The horizontal location of the maximum shear stress at a particular depth moves from a position near the toe of the slope immediately beneath the embankment to the centerline of the embankment at a depth which depends upon the L/H ratio.

A similar trend is shown in Figure 12 for  $\alpha = 30^\circ$ . However, in Figure 13 ( $\alpha = 45^\circ$ ), the largest shear stress occurs near the toe of the slope for L/H = 0.0. Although the smallest L/H ratio shown in Figures 14 and 15 is 0.5, the development of large shear stress near the toe of narrow steep embankments is clearly indicated.

The dashed line in Figure 13 shows the magnitude of the maximum  $\tau_{\max}$  as a function of depth for the normal loading approximation corresponding to the  $45^\circ$  embankment for which L/H = 1. It is evident that the peak magnitudes are nearly the same for the two cases, but it occurs at approximately twice the depth in the case of the normal loading approximation. A similar effect is evident in Figure 10 for L/H = 3. Thus the influence of the elastic embankment is more pronounced nearer the surface where softer soils might be expected. As a result, it may be that current estimates of stability, potential creep and other shear stress related phenomena, for soils at shallow depths beneath embankments, are unconservative.

#### Relationship of Results to In-situ Stresses

It is not immediately clear what relationship these results have to stresses which actually exist in the field. In the case of a built-up



embankment, it is likely that the embankment material will exhibit significantly different mechanical properties from the foundation material. For a cut-down slope, the assumption of homogeneity in the two zones may be more nearly justified. The non-linearity in the mechanical response of most natural materials will undoubtedly also influence the results. However, the feature which may be most significant, at least in the case of built-up embankments, is the fact that they are constructed in layers rather than instantaneously. Thus when the topmost lift is placed on an earth embankment, the upper material does not undergo strain due to elastic deformation of the embankment resulting from the stresses imposed by the entire mass. Rather, the strains are due only to the increment of stress imposed by this layer. The degree to which the results would be changed is not clear. However, it is believed that the results presented herein, provide a more realistic estimate of stress conditions than that computed from the normal loading approximation.

#### Effect of Results on Stress Path Determination

LAMBE (1964) has suggested that the "stress path" method for prediction of vertical settlements of cohesive soils is superior to conventional analyses in cases where compression is clearly not one-dimensional. This approach involves three basic steps (LAMBE, 1964):

1. Estimation of the effective stress path of an "average" element in the compressible layer, for the field loading.
2. Performance of a laboratory compression test which duplicates, insofar as practicable, the field effective stress path.
3. Computation of settlement by multiplying the thickness of the layer considered by the axial (vertical) strain from the laboratory test.

Because the strains in the laboratory sample depend upon the applied stresses, the method requires a means of correctly assessing the in-situ stresses.

A comparison of the total stress paths for several points under the center line of an elastic embankment ( $\alpha = 30^\circ$ ,  $L/H_{\text{final}} = 0.5$ ,  $\mu = 0.3$ ), with those computed using the normal loading approximation, is shown in Figure 16. The dashed "initial stress" line shows the state of stress in an elastic half-space, for which  $\mu = 0.3$ , before construction of the embankment. The three points shown on the line correspond to the stress states depths of 0.5, 1.0 and 2.0 times the final height of the embankment,  $H_{\text{final}}$ . The open points show the stress paths during "construction" of an elastic embankment continuous with the foundation material. The solid points show the stresses for corresponding embankment heights, determined by the conventional method. Several features of this comparison are especially noteworthy:

1. At relatively shallow depths ( $y/H = 0.5$ ), the conventional method leads to a total stress path which lies entirely below the  $k_0$  line. That is, one would predict relatively small shear settlements. However, on the basis of the elastic embankment analysis, the estimated shear induced settlement would likely be larger, and compression settlement would be less.
2. At greater depth ( $y/H_{\text{final}} = 2.0$ ) both methods lead to stress paths which lie above the  $k_0$  line. The two paths are closer, and the shear stress under the elastic embankment is actually less than that due to the normal loading approximation.
3. At intermediate depths ( $y/H_{\text{final}} = 1.0$ ) the normal loading approximation remains relatively close to the  $k_0$  line. The stress path due to the elastic embankment is still considerably steeper.

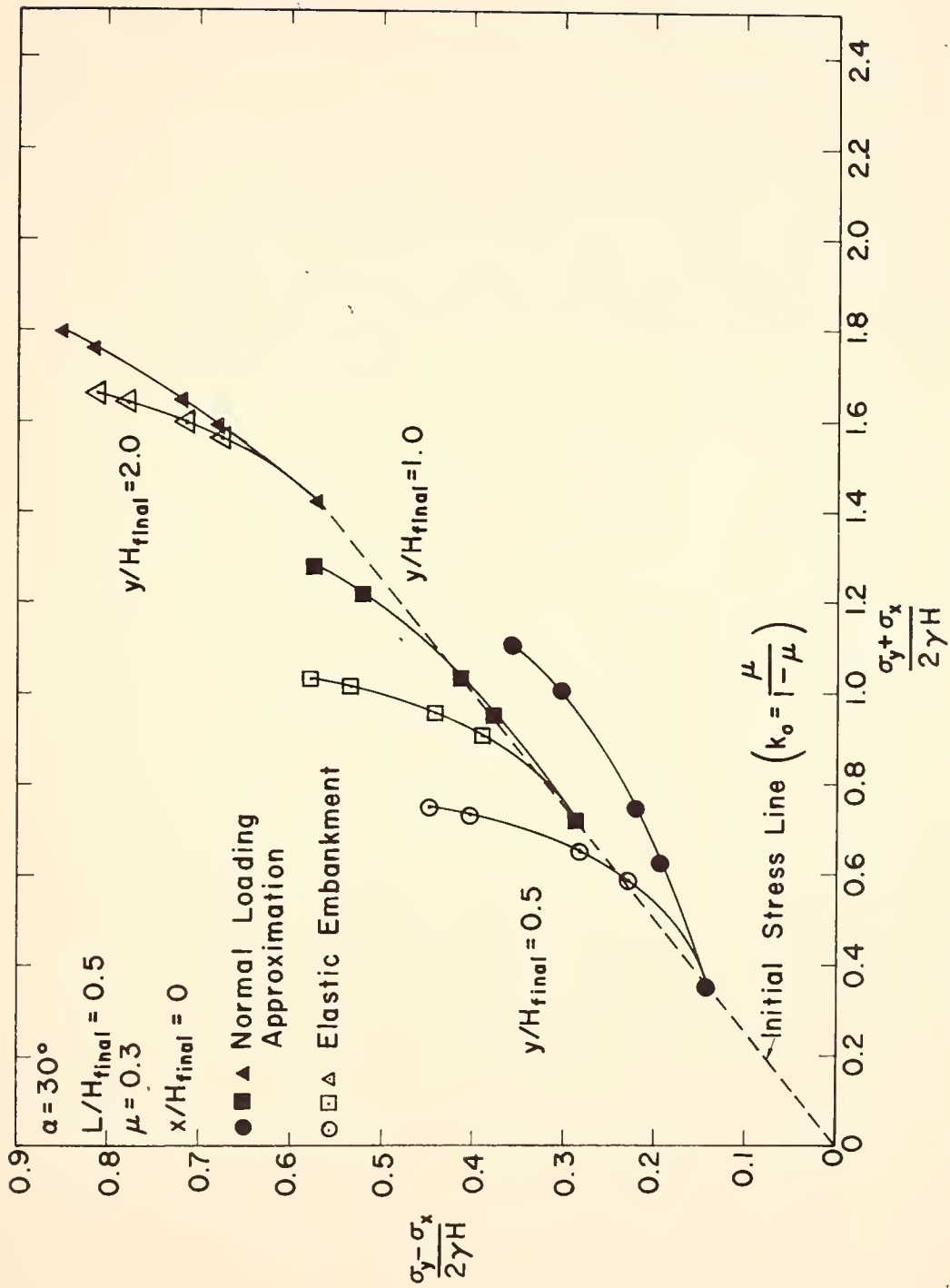


Figure 16 - Stress Path for Three Points Under The Center Line During Embankment Construction

Because of the influence of the applied stress path on the measured laboratory settlements, and therefore on the computed field settlements, it would seem essential to estimate the predictive capability of the method to the field stresses accurately. In the case considered, the stresses produced by the elastic embankment are significantly different from those due to the normal loading approximation, at least at shallow depths. The effect of this difference on the results predicted by the stress path method is not obvious, however this question would appear to deserve further attention.



## CONCLUSIONS

The analysis presented herein permits determination of the stresses within and under long elastic embankments which are continuous with the underlying foundation material. The results indicate that the horizontal distribution of vertical stress is more nearly uniform than is usually assumed. Thus, differential settlements computed using the normal loading approximation will be larger than those determined using the stress distributions presented herein.

The horizontal vertical shear stresses created in the foundation material by the embankment, are found to be significantly higher at shallow depths for the elastic embankment than for the normal loading approximation.

The influence diagrams presented, provide the designer with what is believed to be a more realistic estimate of the vertical stresses than that usually employed.

## ACKNOWLEDGMENTS

The research described herein was supported in part by the Ohio Department of Highways in conjunction with the U. S. Bureau of Public Roads, and in part by the Joint Highway Research Project, Purdue University in conjunction with the U. S. Bureau of Public Roads. The assistance of W. L. DeGroff, R. Hockema, and R. Corbett in the preparation of the drawings is gratefully acknowledged.

## REFERENCES CITED

- BROWN, C. B., (1962) "Incremental Analysis of Gravitational Stresses in Embankments and Their Effect Upon the Failure of Earth Structures," Ph. D. Dissertation, University of Minnesota.
- CARLTON, T. A., Jr., (1962), "The Distribution of Gravity Stresses in a Symmetrical Trapezoidal Embankment and its Foundation," Ph. D. Thesis, University of Texas, 1962.
- CAROTHERS, S. D., (1920), "Direct Determination of Stresses," Proceedings, The Royal Society of London, Series A., Vol. XCVII, p. 110.
- CHURCHILL, R. V., (1948), Introduction to Complex Variables and Applications, McGraw-Hill Book Company, Inc., New York.
- CLOUGH, R. and CHOFRÁ, A. K., (1966) "Earthquake Stress Analysis in Earth Dams," Journal of the Engineering Mechanics Division, Proceedings ASCE, Vol. 92, No. EU2, April, 1966.
- DAVIS, E. H. and TAYLOR, H., "The Movement of Bridge Approaches and Abutments on Soft Foundation Soils," Paper No. 37, Proceedings Australian Research Board, Part 2, Vol. 1, 1962.
- DINGWALL, J. C. and SCRIVNER, F. H., (1954) "Application of the Elastic Theory to Highway Embankments by Use of Difference Equations," Proceedings, Highway Research Board, v. 33, p. 474.
- FINN, W. D. L., (1960) "Stresses in Soil Masses Under Various Boundary Conditions," Ph. D. Thesis, University of Washington, 1960.
- FINN, W. D. L., (1966) "Static and Dynamic Stresses in Slopes," Proceedings, of the First Congress of the International Society of Rock Mechanics, V. II, p. 167.
- GOODMAN, L. E. and BROWN, C. B., (1963) "Dead Load Stresses and Instability of Slopes," Journal of the Soil Mechanics and Foundations Division, Proceedings ASCE, V. 89, n SM3, May 1963.
- HENDERSON, F. M., (1960) Elliptic Functions with Complex Arguments, University of Michigan Press, Ann Arbor.
- HILDEBRAND, F. B., (1956) Introduction to Numerical Analysis, McGraw-Hill, New York.
- JURGENSON, L. (1937) "The Application of Theories of Elasticity and Plasticity to Foundation Problems," Journal of the Boston Society of Civil Engineers, July, 1934.
- LAMBE, T. W., (1964) "Methods of Estimating Settlement", Proceedings of the ASCE Conference on Design of Foundations for Control of Settlement, p. 47.

- MUSKHELISHVILI, N. I., (1953) Some Basic Problems of the Mathematical Theory of Elasticity, P. Noordhoff, Groningen.
- NEWMARK, N. M., (1940) "Stress Distribution in Soils," Proceedings Purdue Conference on Soil Mechanics and its Applications, p. 295.
- NEWMARK, N. M., (1942) "Influence Charts for Computation of Elastic Stresses in Foundations," Bulletin, University of Illinois Engineering Experiment Station, No. 338.
- OSTERBERG, J. O., (1957) "Influence Value for Vertical Stresses in a Semi-Infinite Mass Due to an Embankment Loading," Proceedings of the Fourth International Conference on Soil Mechanics and Foundation Engineering, Vol. I, p. 393.
- RENDULIC, L., (1938) "Der Erddruck im Strassenbau und Bruckenbau," Forschungsberb. Strassenwesen, Bd. 10, Volk u. Reich Verlag, Berlin.
- TERZAGHI, K., (1943) Theoretical Soil Mechanics, John Wiley, New York.
- TIMOSHENKO, S. and GOODIER, J. N., (1951) Theory of Elasticity, McGraw-Hill, New York.
- TROLLOPE, D. H., (1957) "The Systematic Arching Theory Applied to Stability Analysis of Embankments," Proceedings 4th International Conference on Soil Mechanics and Foundation Engineering, V. 2, p. 382.
- WYLIE, C. R., Jr., (1966) Advanced Engineering Mathematics, Third Edition, McGraw-Hill, New York.
- ZIENKIEWICZ, O. C., (1947) "Stress Distribution in Gravity Dams," Journal of the Institution of Civil Engineers, V. 27, January 1947, p. 247.
- ZIENKIEWICZ, O. C. and CHEUNG, Y. K., (1964) "Buttress Dams on Complex Rock Foundations," Water Power, Vol. 16, No. 5, May 1964, p. 193.
- ZIENKIEWICZ, O. C. and CHEUNG, Y. K., (1965) "Stresses in Buttress Dams," Water Power, Vol. 17, No. 2, February 1965, p. 69.
- ZIENKIEWICZ, O. C. and GERSTNER, R. W., (1961) "Foundation Elasticity Effects in Gravity Dams," Proceedings of the Institution of Civil Engineers, V. 19, p. 209.



## APPENDIX 1

## SOLUTION OF THE PROBLEM

The method of solution is a modification of the MUSKHELISHVILI (1953) method. A brief outline of the solution is given below. A more complete discussion of the details will be presented in a forthcoming paper.

For the plane strain problem, the stresses can be defined in terms of an Airy stress function,  $U(x,y)$  as:

$$\begin{aligned}\sigma_x &= \frac{\partial^2 U(x,y)}{\partial y^2} + \frac{\mu}{1-\mu} \gamma y \\ \sigma_y &= \frac{\partial^2 U(x,y)}{\partial x^2} + \gamma y \\ \tau_{xy} &= - \frac{\partial^2 U(x,y)}{\partial x \partial y}\end{aligned}\tag{1}$$

where  $\sigma_x$ ,  $\sigma_y$ ,  $\tau_{xy}$  are the horizontal normal, vertical normal and shear stress, respectively,  $\gamma$  is the unit weight of the material,  $\mu$  is the Poisson's ratio. For a case in which weight is the only body force acting, the requirements of equilibrium and compatibility will be satisfied if (TIMOSHENKO and GOODIER, 1951):

$$\nabla^4 U(x,y) = 0\tag{2}$$

where  $\nabla^2$  is the Laplacian operator.

When the boundary conditions of the specific problem are also satisfied, the unique solution has been obtained.

In considering the boundary conditions associated with the embankment, it is convenient to represent the Airy stress function in complex



form. Referring to the plane in which the embankment section is shown in Figure 1b, as the  $z$ -plane, a point within the medium can be represented by the complex number,  $z = x + iy$ . Assuming that the stress function is analytic within the medium, the function can be written as:

$$U(x,y) = \text{Re} \left[ \bar{z}\phi(z) + \chi(z) \right] \quad (3)$$

where  $\bar{z} = x - iy$ ,  $\phi$  and  $\chi$  are single-valued analytic functions throughout the  $z$ -plane. The functions  $\phi$  and  $\chi$  are determined from the conditions that the normal and tangential stresses on the boundary are equal to zero. Substituting Equation 3 into Equations 1, and expressing the stresses in terms of the boundary tractions leads to:

$$\begin{aligned} N + iT = \phi'(z) + \overline{\phi'(\bar{z})} - e^{2i\theta} \left[ \bar{z}\phi''(z) \right. \\ \left. + \chi'(z) + \frac{\gamma y}{2} \left( \frac{1-2\mu}{1-\mu} \right) \right] + \frac{\gamma y}{2} \left( \frac{1}{1-\mu} \right) \end{aligned} \quad (4)$$

where a bar indicates the complex conjugate of the quantity,  $\theta$  is the angle between the slope and the  $x$ -axis measured in a clockwise direction,  $\mu$  is Poisson's ratio,  $N$  and  $T$  are the normal and tangential components, respectively, of the boundary traction.

Evaluation of the stresses is then accomplished by a two step transformation. First, the boundary of the  $z$ -plane is transformed into the straight line boundary of an auxiliary plane, the  $t$ -plane,  $t = \xi + i\eta$ , by the application of the Schwarz-Christoffel transformation (CHURCHILL, 1948):

$$z = f(t) = R \int_0^t \left( \frac{1 - \beta^2 \lambda^2}{1 - \lambda^2} \right)^{\frac{1}{2}} d\lambda + S \quad (5)$$

where R and S are constants,  $\beta$  is the modulus,  $\lambda$  is a dummy variable and  $n = \pi/\alpha$ . Note that when  $n = 2$ , corresponding to a slope angle of  $90^\circ$ , the integral expression in Equation 5 is an elliptic integral of the second kind, for which tables or charts (HENDERSON, 1960) are available. For those cases where  $n$  is larger than 2, the integral can be evaluated numerically on the computer. In this analysis, Equation 5 was evaluated for all values of  $n$  on the IBM 7094 digital computer by a Simpson's rule integration (HEIDBRAND, 1956).

Because Equation 5 represents a conformal transformation, straight lines  $\xi = \text{constant}$  and  $\eta = \text{constant}$  in the  $t$ -plane, correspond to orthogonal curvilinear coordinates in the  $z$ -plane. This is illustrated in Figure A.1a. Thus, the boundary conditions in terms of  $\phi(z)$  and  $\chi(z)$  can be written as functions of  $\phi [f(t)] = \phi(t)$  and  $\chi [f(t)] = \chi(t)$ . Then the boundary tractions become:

$$N + iT = 0 = \dot{\Phi}(t) + \overline{\dot{\Phi}(t)} + \frac{\gamma}{2(1-\mu)} \text{Im} [f(t)] \\ + \frac{f'(t)}{f'(t)} \left[ \overline{f(t)} \frac{\dot{\Phi}'(t)}{f'(t)} + \dot{\Psi}(t) + \frac{\gamma}{2} \left( \frac{1-2\mu}{1-\mu} \right) \text{Im} [f(t)] \right] \quad (6)$$

where  $\dot{\Phi}(t) = \phi'(t)$ ,  $\dot{\Psi}(t) = \chi'(t)$  and  $f'(t)$  is the integrand of Equation 5. Recognizing  $\eta = 0$  and  $t = \xi$  in Equation 6, and rearranging leads to:

$$\dot{\Phi}(\xi) + \overline{\dot{\Phi}(\xi)} + \frac{f'(\xi)}{f'(\xi)} \left[ \overline{f(\xi)} \frac{\dot{\Phi}'(\xi)}{f'(\xi)} + \dot{\Psi}(\xi) \right] = \\ \frac{\gamma}{2(1-\mu)} \left[ 1 + (1-2\mu) \frac{f'(\xi)}{f'(\xi)} \right] \text{Im} [f(\xi)] \quad (7)$$

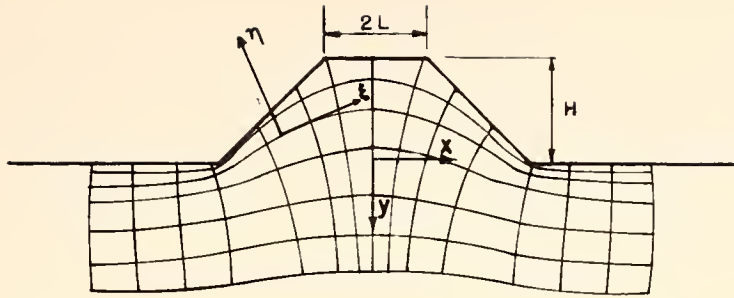
In this form, Equation 7 expresses the effect in the  $t$ -plane of the geometric shape of the embankment. This effect can be visualized as a "fictitious loading" applied to the boundary of the  $t$ -plane. The real and imaginary parts of this "fictitious boundary loading" are shown in Figures A.1b and A.1c, respectively.

Having expressed the desired functions of the boundary, it is necessary to determine them inside the boundary. This is accomplished by the application of the Cauchy integral formula. This formula states that for a given function  $g(\xi)$  along a closed contour,  $C$ , which satisfies certain conditions, the value of the function at an interior point,  $t$ , is (WYLIE, 1966):

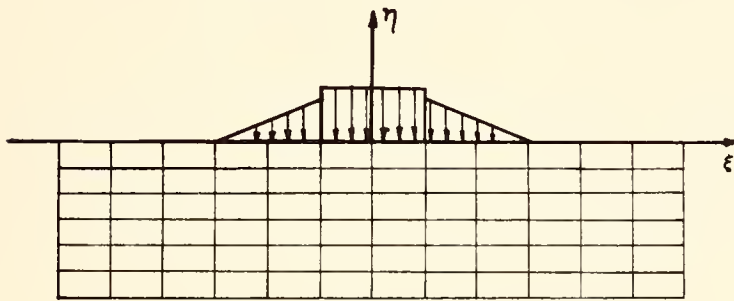
$$g(t) = \frac{1}{2\pi i} \int_C \frac{g(\xi)}{\xi - t} d\xi \quad (8)$$

If the point  $t$  is exterior to the closed contour, then the integral expression equals zero. By this means, the desired functions can be evaluated inside the boundary. Knowing  $\bar{\Phi}(t)$  and  $\bar{\Psi}(t)$ , and substituting Equation 3 into Equations 1, leads to the determination of the stresses:

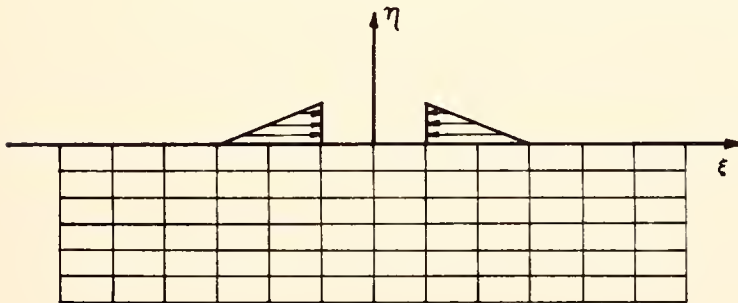
$$\begin{aligned} \sigma_x &= 2 \operatorname{Re} \bar{\Phi}(t) - \operatorname{Re} \left[ \bar{f}(t) \frac{\bar{\Phi}'(t)}{\bar{f}'(t)} + \bar{\Psi}(t) \right] + \left( \frac{\mu}{1-\mu} \right) \gamma \operatorname{Im} [f(t)] \\ \sigma_y &= 2 \operatorname{Re} \bar{\Phi}(t) + \operatorname{Re} \left[ \bar{f}(t) \frac{\bar{\Phi}'(t)}{\bar{f}'(t)} + \bar{\Psi}(t) \right] + \gamma \operatorname{Im} [f(t)] \\ \tau_{xy} &= \operatorname{Im} \left[ \bar{f}(t) \frac{\bar{\Phi}'(t)}{\bar{f}'(t)} + \bar{\Psi}(t) \right] \end{aligned} \quad (9)$$



(a) Geometrical Transformation



(b) Transformation of "Fictitious Stresses" on Boundary-Real Part



(c) Transformation of "Fictitious Stresses" on Boundary- Imag. Part

Fig.A.I - Graphical Representation of Transformation Procedure



## APPENDIX 2

This Appendix contains influence diagrams for vertical normal stress and horizontal normal stress along vertical sections for  $\mu = 0.3$ ,  $\alpha = 15^\circ$ ,  $30^\circ$ ,  $45^\circ$ ,  $60^\circ$  and  $75^\circ$ , and various embankment shapes. Influence diagrams for horizontal and vertical shear stress for  $\alpha = 45^\circ$ ,  $\mu = 0.3$  and various embankment shapes are also given.

The diagrams indicate the stress due to the embankment weight alone. Stresses due to the weight of material underlying the embankment must be superimposed to obtain the total stress. The stresses are expressed in dimensionless form as  $\sigma_y/\gamma H$ ,  $\sigma_x/\gamma H$  or  $\tau_{xy}/\gamma H$ . The coordinates are also in dimensionless form. For convenience in the semi-logarithmic plot, the depth is measured from the top of the embankment, and designated  $\bar{y}/H$ . This is in contrast to the discussion in the body of the paper where the vertical distances are measured from the base of the embankment and designated  $y/H$ .

Each of the four diagrams in a given figure refers to a particular vertical section, shown schematically on the diagram. The upper left diagram indicates stresses along a vertical section midway between the centerline and the toe of the slope; the lower left diagram indicates stresses along a vertical section through the toe of the slope; the lower right diagram indicates stresses along a vertical section located a distance from centerline equal to 1.5 times the distance from the centerline to the toe of the slope.



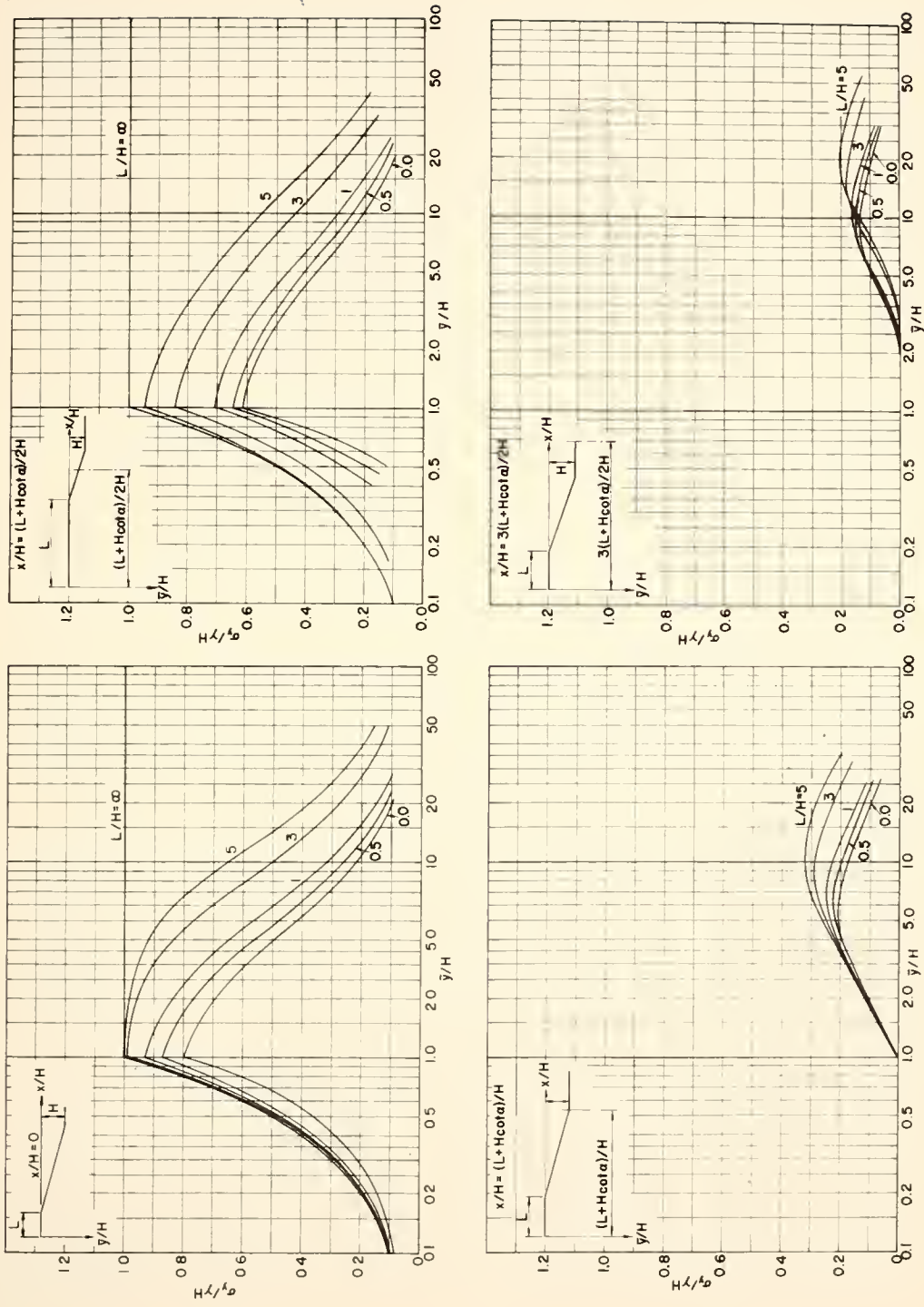


Fig. A.2-Influence Diagrams for Vertical Normal Stress Along Selected Vertical Sections for  $\alpha = 15^\circ$ ,  $\mu = 0.3$

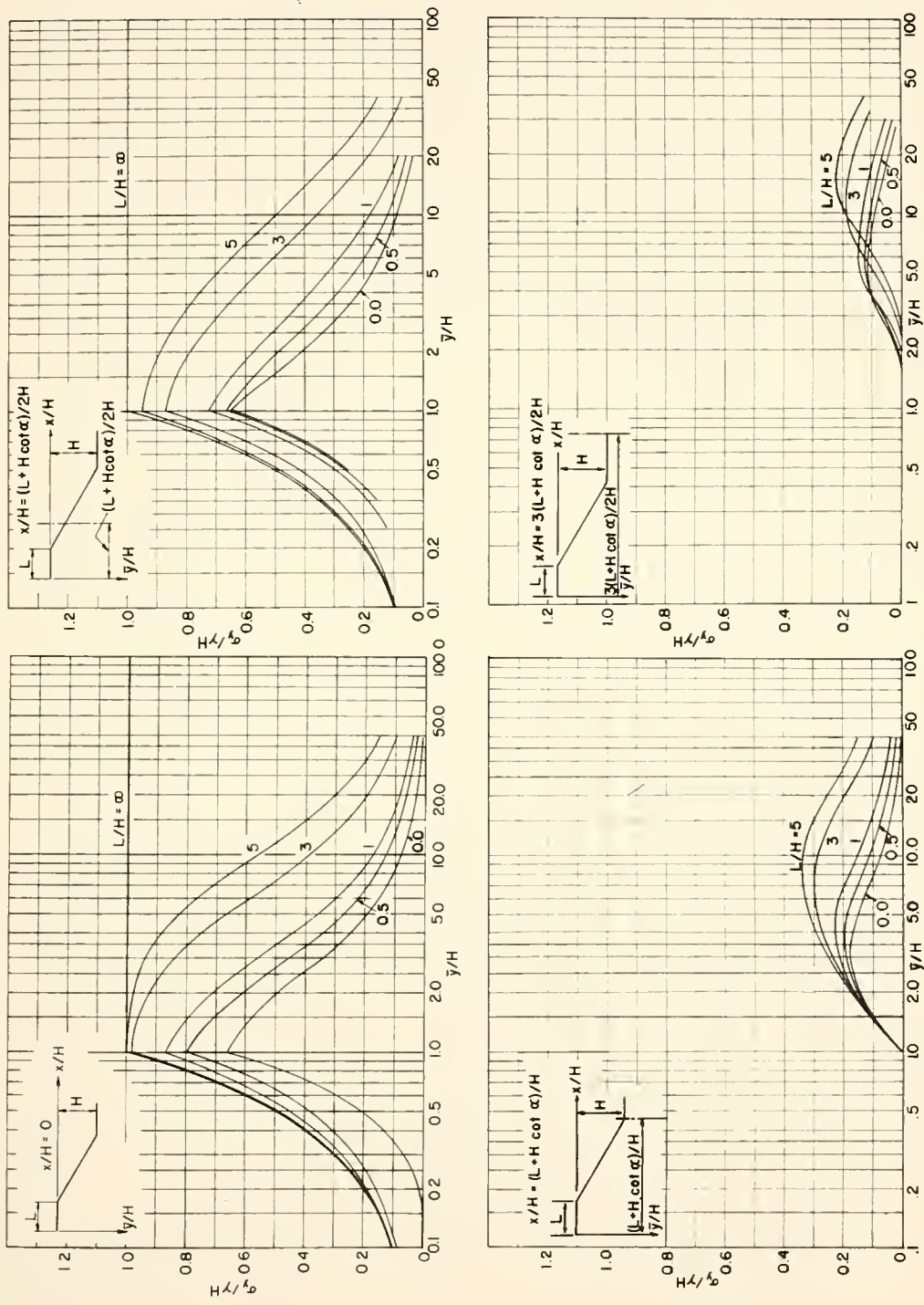


Fig.A.3-Influence Diagrams for Vertical Normal Stress Along Selected Vertical Sections for  $\alpha = 30^\circ$ ,  $\mu = 0.3$

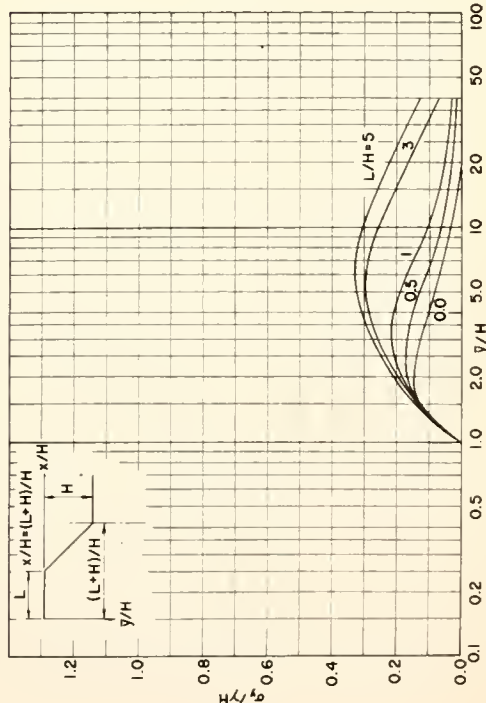
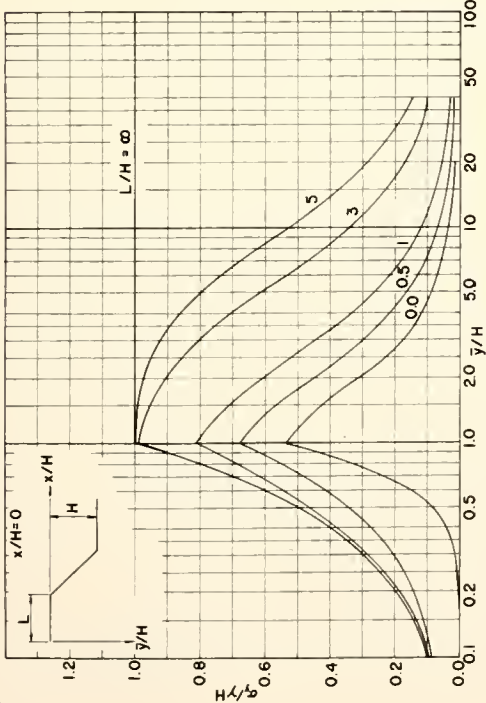
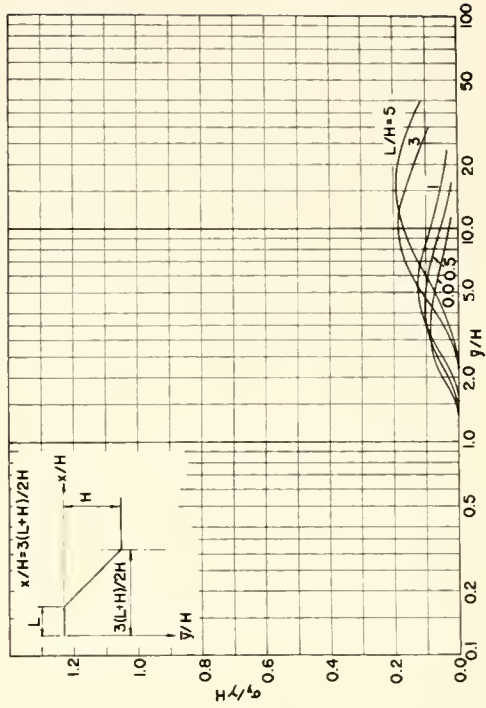
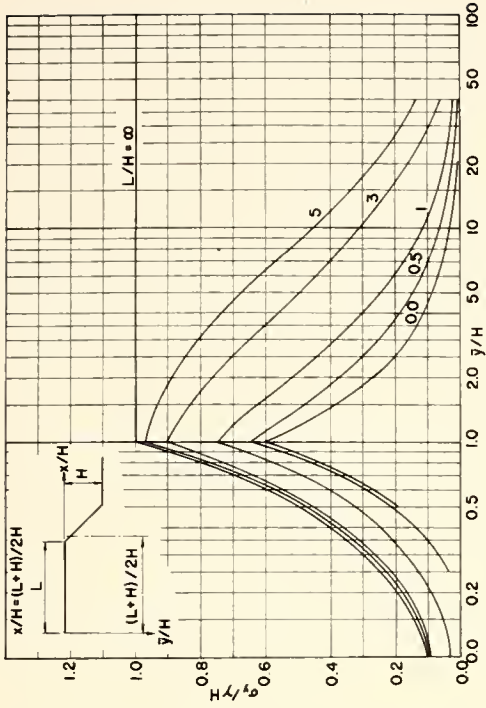


Fig. A.4-Influence Diagrams for Vertical Normal Stress Along Selected Vertical Sections for  $\alpha = 45^\circ$ ,  $\mu = 0.3$

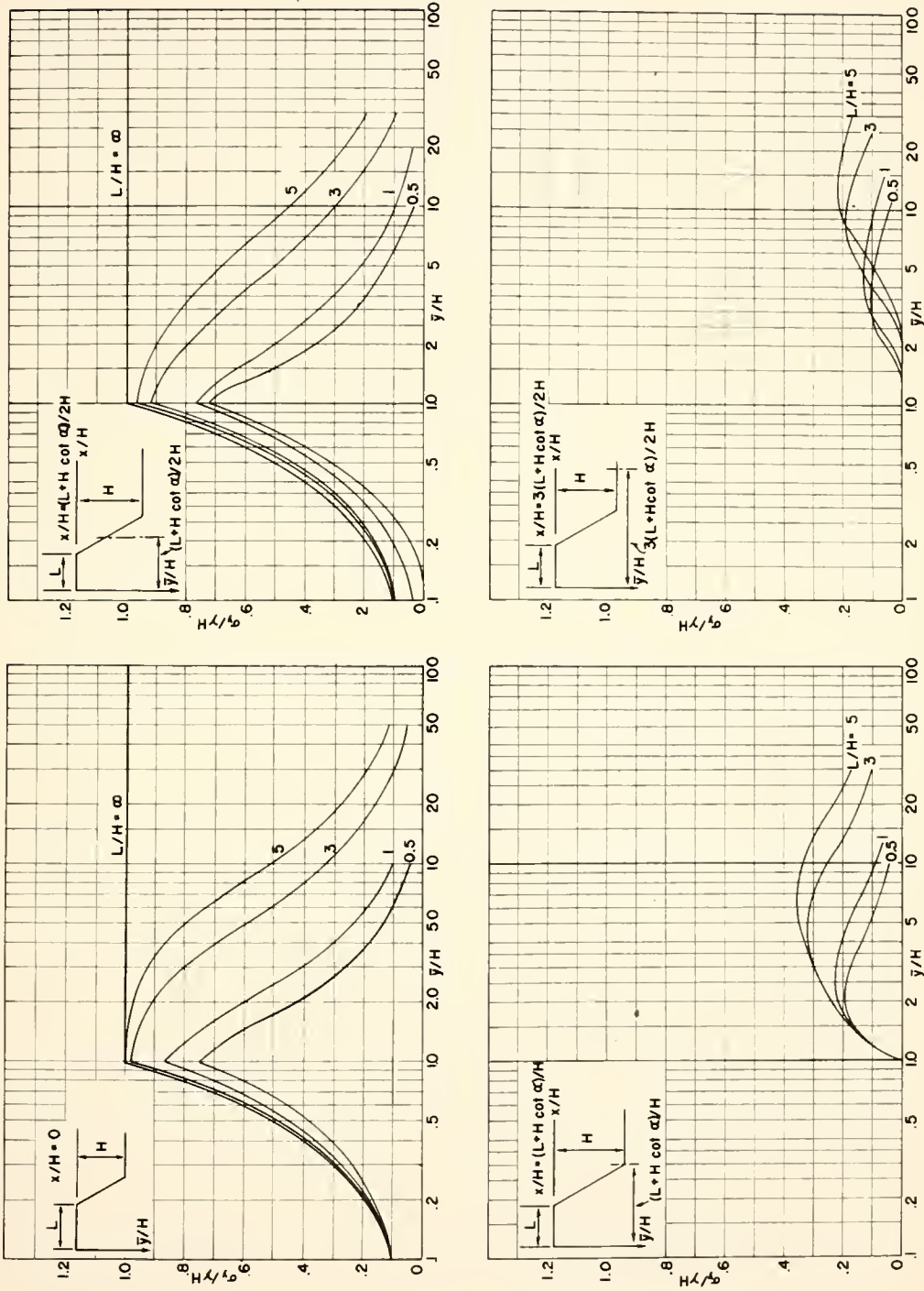


Fig.A.5-Influence Diagrams for Vertical Normal Stress Along Selected Vertical Sections for  $\alpha = 60^\circ$ ,  $\mu = 0.3$



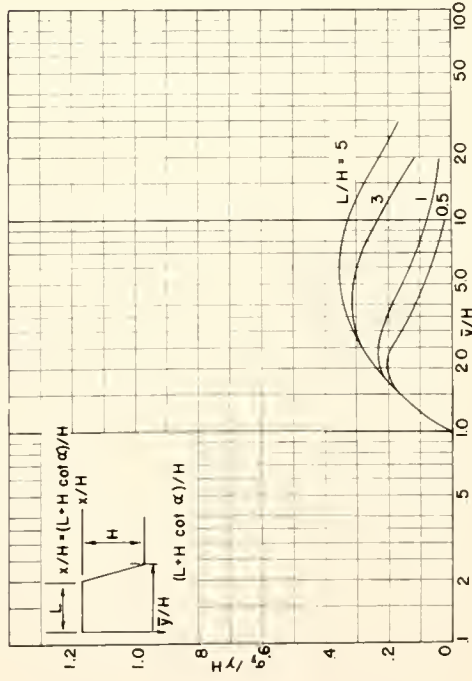
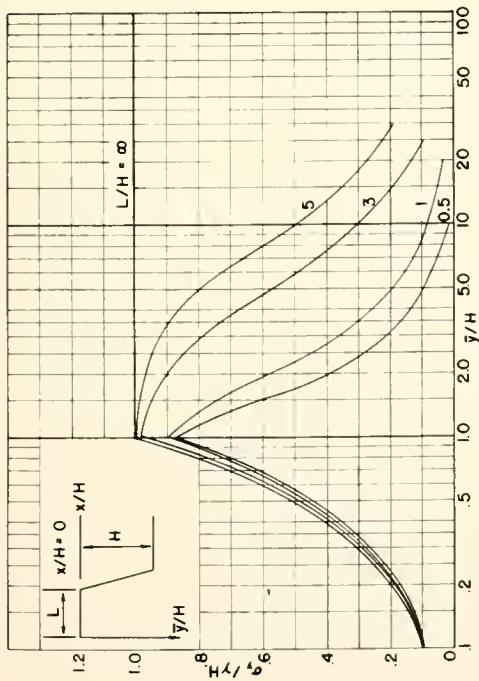
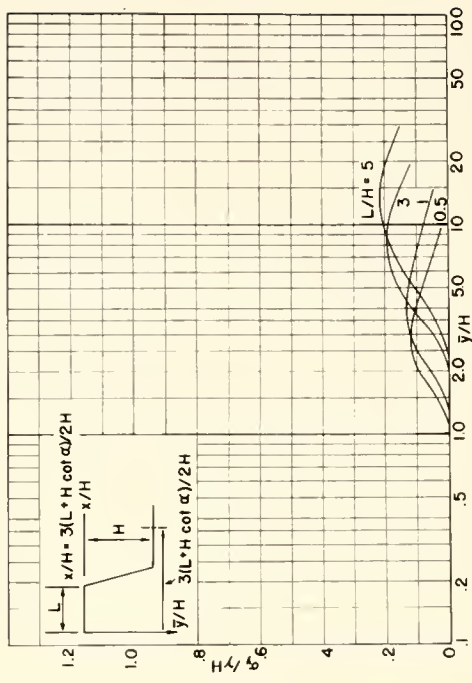
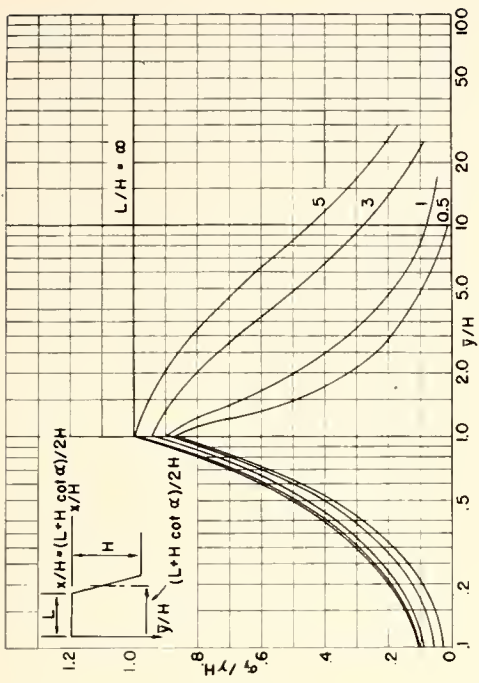


Fig. A.6-Influence Diagrams for Vertical Normal Stress Along Selected Vertical Sections for  $\alpha = 75^\circ$ ,  $\mu = 0.3$



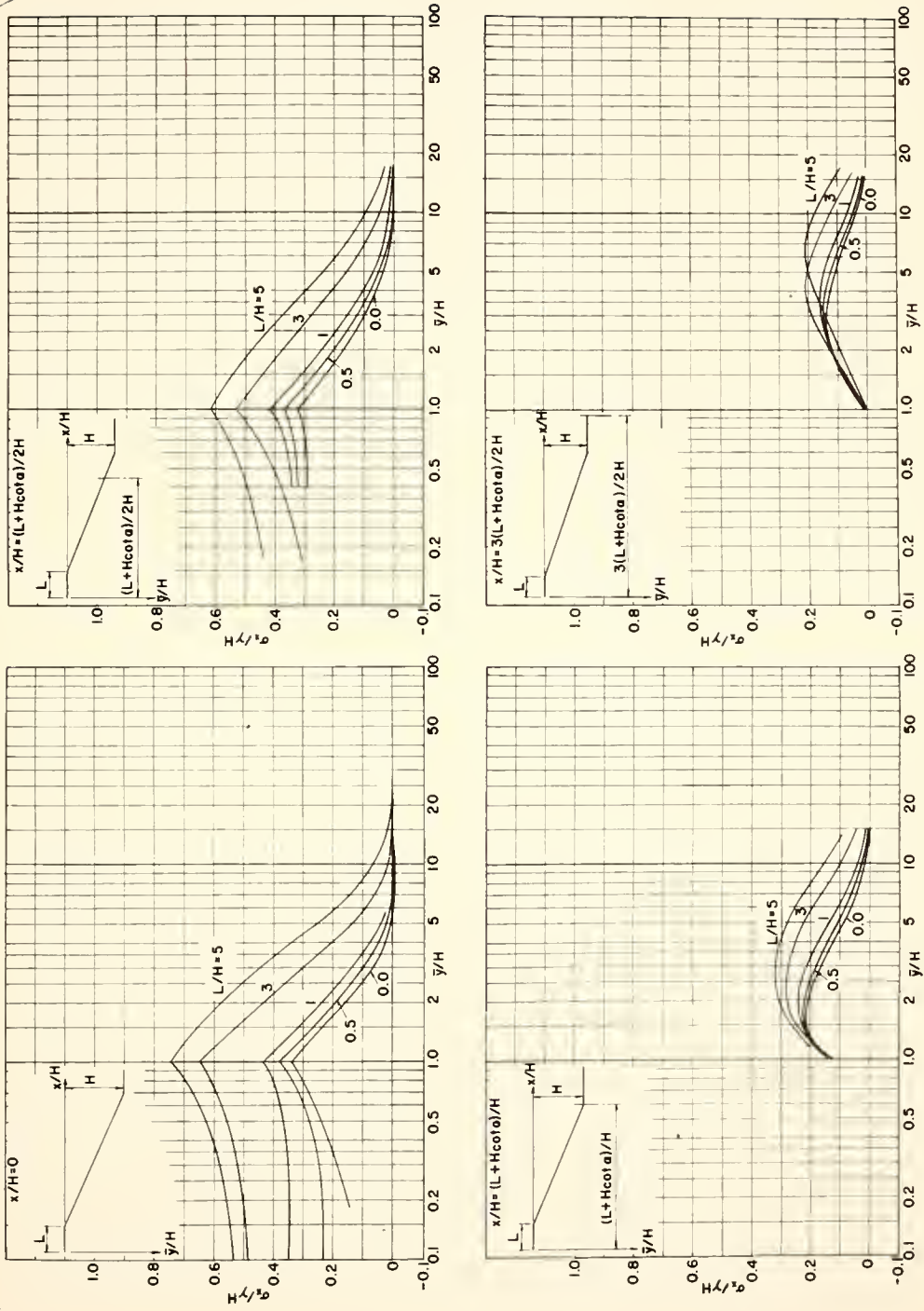


Fig. A.7- Influence Diagrams for Horizontal Normal Stress Along Selected Vertical Sections for  $\alpha = 15^\circ$ ,  $\mu = 0.3$

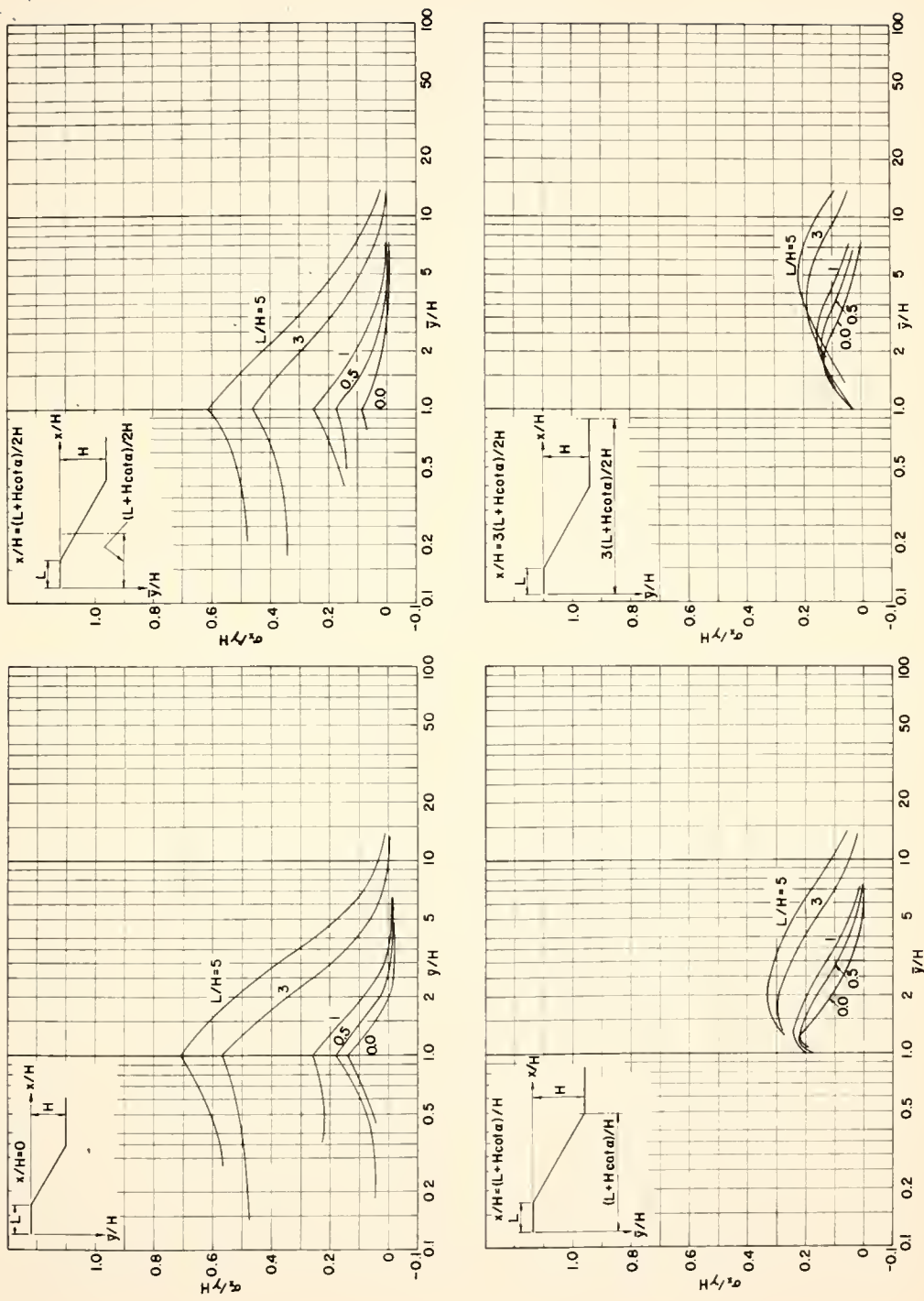


Fig. A.8-Influence Diagrams for Horizontal Normal Stress Along Selected Vertical Sections for  $\alpha = 30^\circ$ ,  $\mu = 0.3$

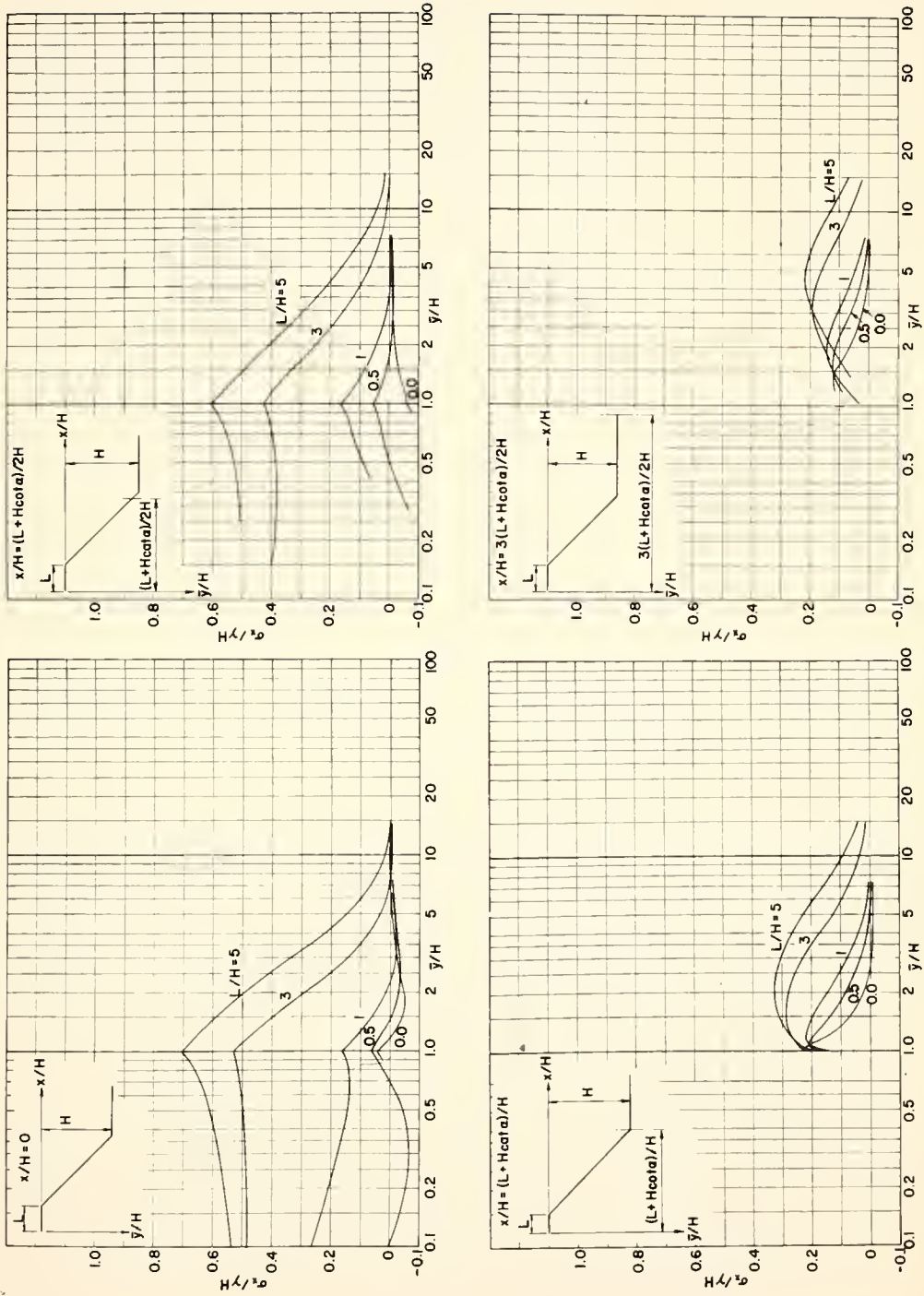


Fig. A.9 - Influence Diagrams for Horizontal Normal Stress Along Selected Vertical Sections for  $\alpha = 45^\circ$ ,  $\mu = 0.3$

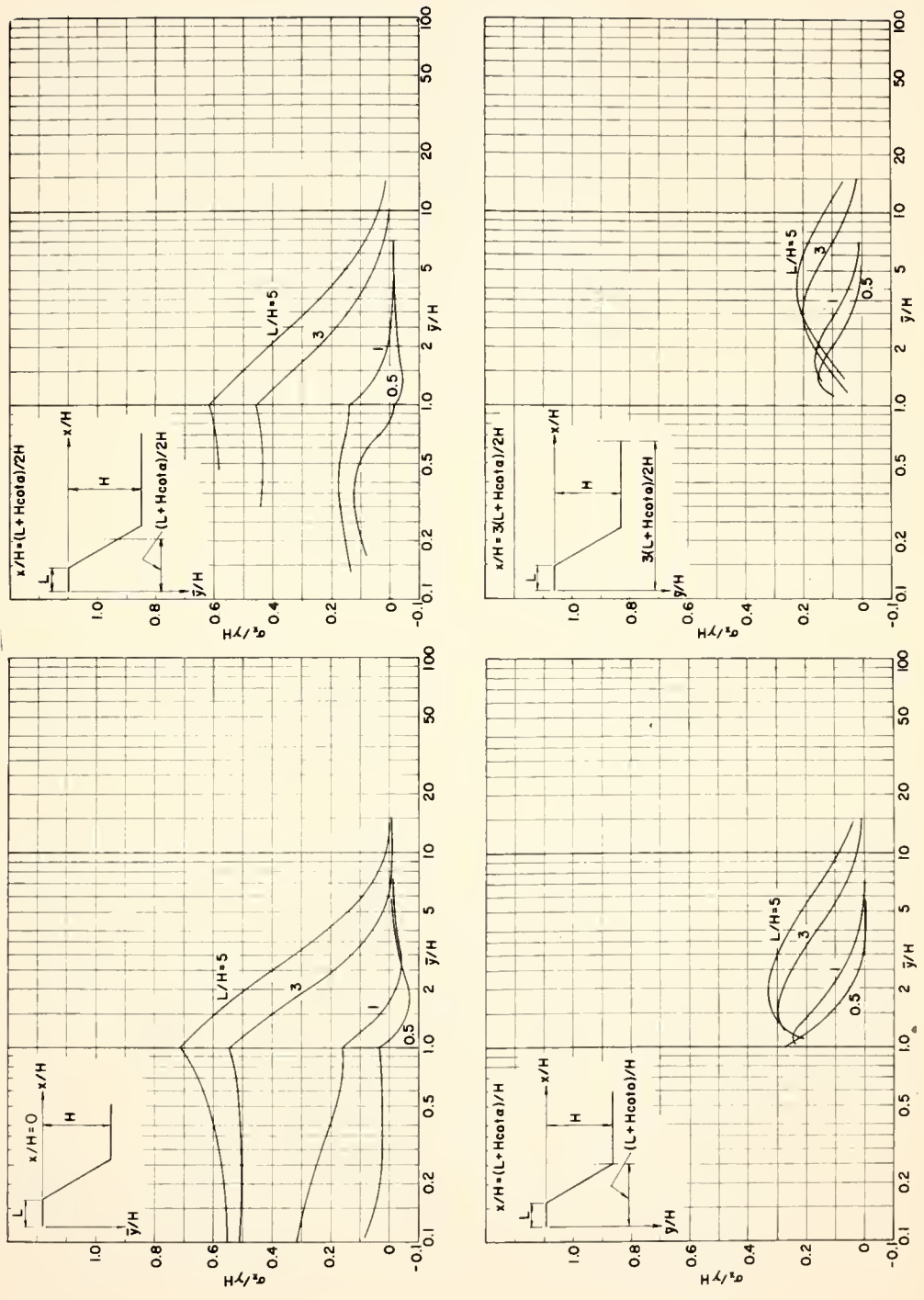


Fig. A.10-Influence Diagrams for Horizontal Normal Stress Along Selected Vertical Sections for  $\alpha = 60^\circ$ ,  $\mu = 0.3$



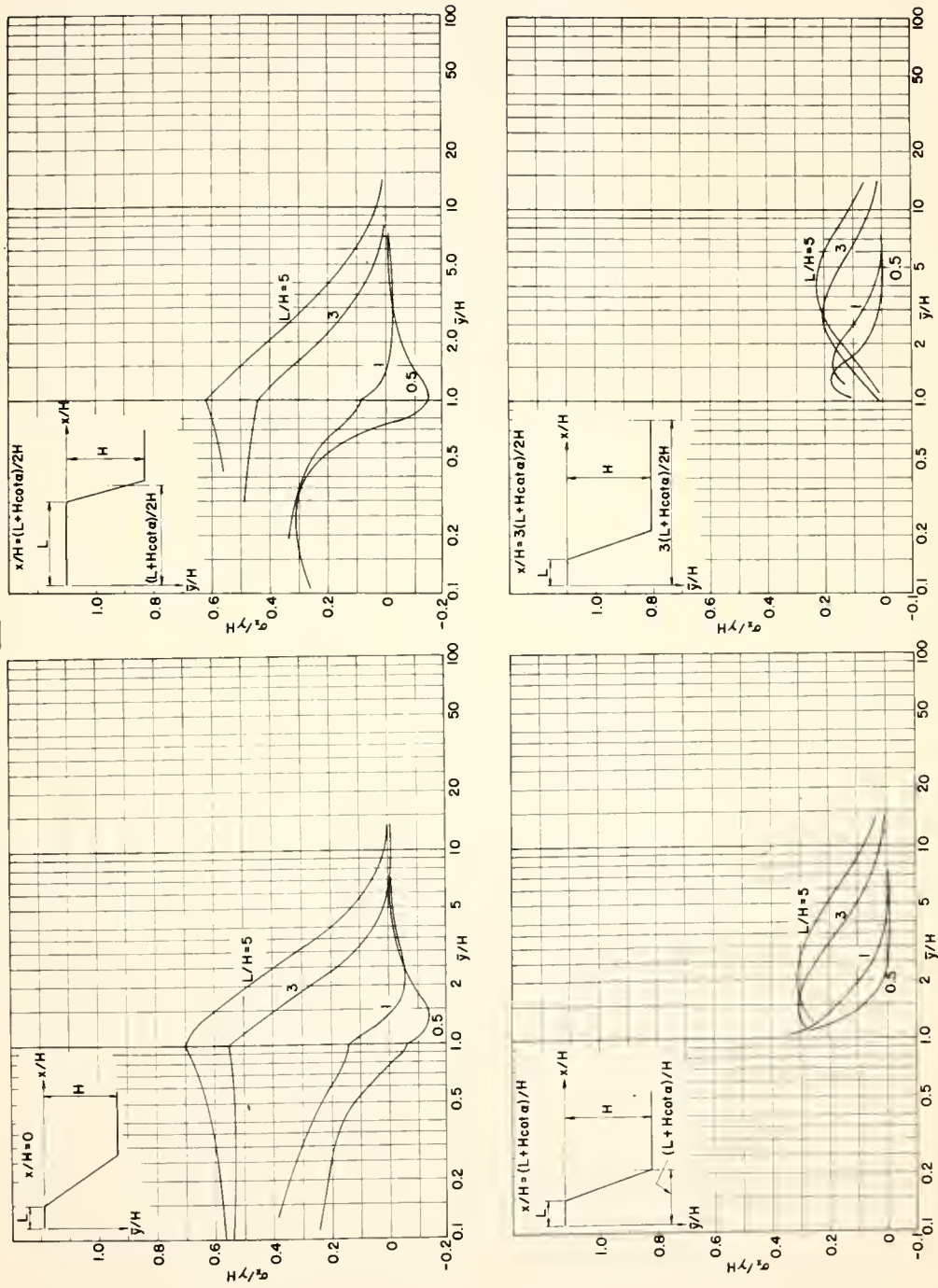


Fig. A.11—Influence Diagrams for Horizontal Normal Stress Along Selected Vertical Sections for  $\alpha = 75^\circ$ ,  $\mu = 0.3$



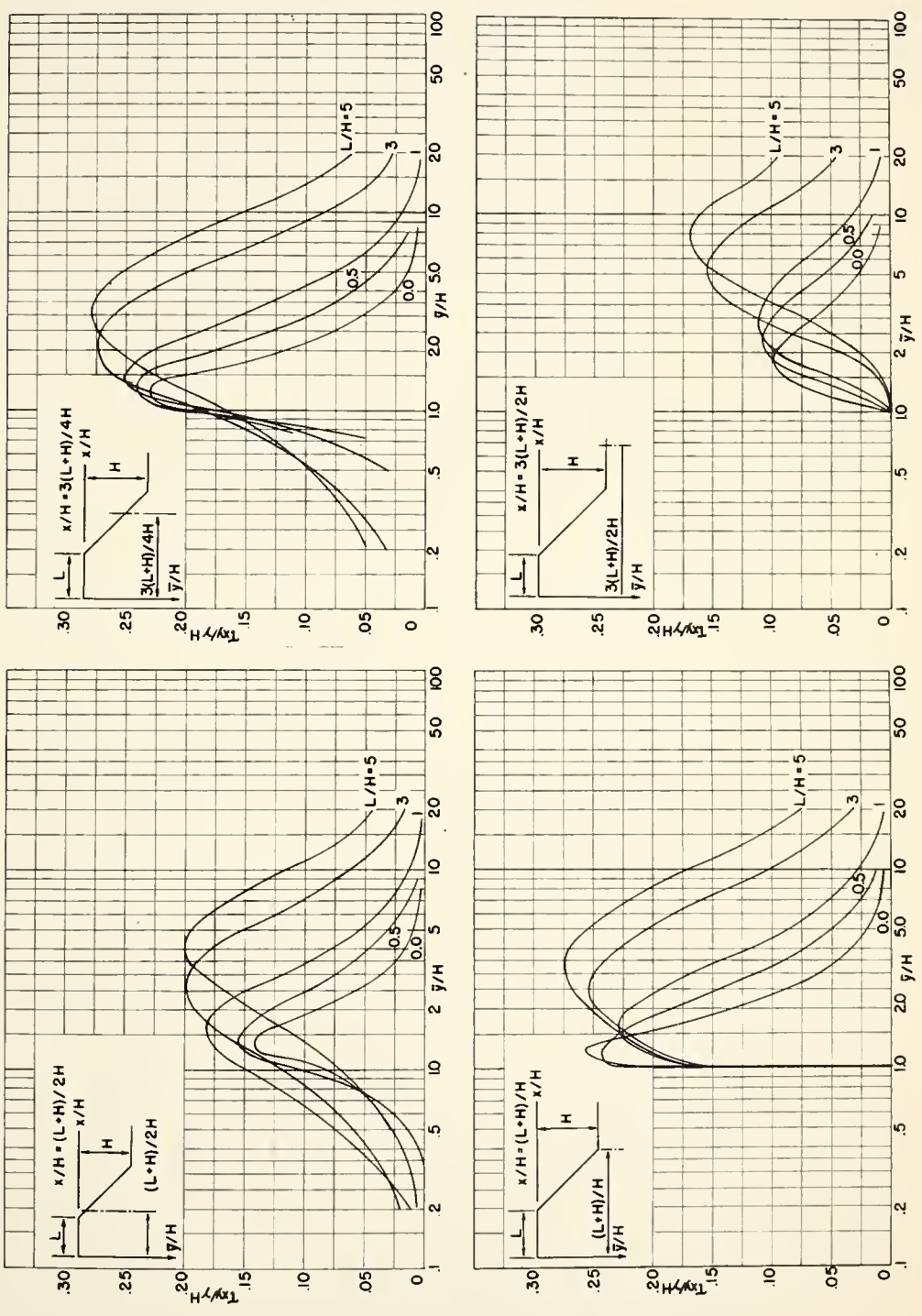


Fig. A.12-Influence Diagrams for Shear Stress Along Selected Vertical Sections for  $\alpha = 45^\circ$ ,  $\mu = 0.3$



